Università degli studi di Padova

Facoltà di Ingegneria

Tesi di Laurea Magistrale in

Ingegneria Elettronica

In collaborazione con

Laboratory for Applied Physics, Università di Verona

Study of the post growth recrystallization of CdTe for the fabrication of low cost high efficiency solar cells.

Relatore

Prof. Gaudenzio Meneghesso

Candidato

Bing Lei Xu

Correlatore

Prof. Alessandro Romeo

Anno Accademico 2013/2014

Contents

List of Figures

List of Tables

Abstract

CdTe thin film solar cells have demonstrated high scalability, high efficiency and low cost fabrication process. One of the key factors for the success of this technology is the transformation of the absorber layer by an activation treatment where chlorine reacts with CdTe in a controlled atmosphere or in air, improving the electrical properties of the absorber, and enhancing the intermixing of the CdS/CdTe layers. At the Laboratory for Applied Physics high efficiency CdTe solar cells are fabricated, exceeding 15% efficiency, with a low temperature process, where all the layers are deposited by vacuum evaporation with temperature below 450°C. The $CdCl_2$ treatment is typically prepared by putting drops of a methanol solution with a specific concentration of $CdCl_2$. Starting from previous work where it was reported the quantity of $CdCl_2$ by changing the methanol concentration and studying the effect of the different amount of $CdCl_2$, I have now analyzed the recrystallization treatment by tuning the annealing temperature from 310°C up to 410°C in air. By doing so we address the multiple effects that this process has on the material and device properties for CdTe solar cells. Activated CdTe layers have been analyzed by means of X-Ray diffraction spectroscopy and atomic force microscopy. A detailed analysis of the formation of intermixed CdS-CdTe layer with temperature will also be reported. Finished devices with efficiencies from 8% for the low temperature annealing up to more than 14% for the high temperature ones, have been thoroughly analyzed by current-voltage, capacitance-voltage and drive level capacitance profiling techniques, showing that carrier concentration is independent with temperature but that a complete different behavior of the defects is reported. A comprehensive overview of the $CdCl_2$ activation treatment will be given.

Chapter 1

CdTe Cell Fabrication Process

Cadmium telluride thin film technology for PV applications is very attractive due to its lower cost of fabrication than the most diffused silicon technology. CdTe devices are made with a stack of thin film deposited on a glass substrate. There are many way to make solar cells with CdTe, using different materials, different deposition techniques or different conditions. This chapter describes the fabrication process developed at Verona University's laboratories. Figure 1.1 shows the structure of CdTe devices.

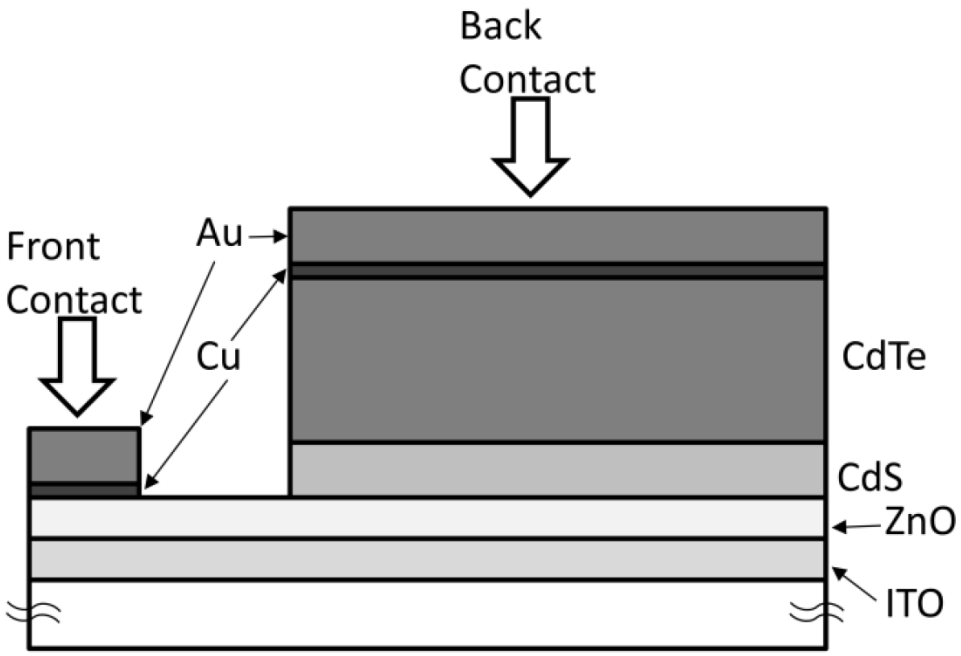

Figure 1.1: CdS/CdTe solar cell structure.

1.1 Front Contact

Electron-hole pairs generated from the absorption of photons must be extracted before they recombine and contacts quality plays an important role on the device performance. Material must be chosen properly in order to have a good ohmic contact, as resistance of contacts and connections may cause significant energy loss.

Solar cells made at our laboratories are in superstrate configuration, so the front contact is the first layer deposited on the glass substrate. Typical sample used in this work has ITO (Indium tin oxide, SnO_2:In_2O_3) as front contact layer because it is highly conductive and very transparent. ITO is deposited by direct current magnetron sputtering, another thin buffer layer of ZnO is stacked on the ITO to avoid indium diffusion. Buffer layer is an insulator so it must be as thin as possible to keep a low vertical resistance but it also has the positive effect to increase shunting resistance of the device. Typical sample front contact is made by 400 nm of ITO and 100 nm of ZnO. After front contact deposition samples are washed by hand with soap, then boiled one hour in milli-ρ water. After that, samples are put in ultrasonic bath with acetone for 20 minutes and isopropanol for 20 minutes more. Samples are dried with argon and put in a vacuum evaporation chamber for CdS deposition.

1.2 CdS window layer

CdS is an n-type semiconductor with energy gap around 2.4 eV. It is usually called window layer or buffer layer because light absorbed by CdS is lost; it is commonly assumed that the hole diffusion length L_p in CdS is very small and thickness cannot be reduced too much because voids in this layer may shunt the absorber layer with the front contact. Moreover one of the activation treatment effect is to cause interdiffusion between CdS and CdTe, and CdS should not be entirely consumed by intermixing (see paragraph 1.4). Energy bands of window layer and absorber layer should be more or less matched, the misalignment of the conduction band (CB) is determined by the electron affinity of both materials: $\Delta E_C = \chi^{CdS} - \chi^{CdTe}$. In case of a too positive ΔE_C band diagram shows a cliff and may cause a loss in the open circuit voltage V_{oc}, while in case of a too negative ΔE_C we have a spike in the band diagram that could reduce short circuit current density J_{sc} see figure 1.2. Electron affinity of pure materials are $\chi^{CdS} = 4.5$ eV and $\chi^{CdTe} = 4.28$ eV, giving a small cliff of 0.22 eV. Due to scatter in the reported χ values in literature and the intermixing phase between CdS and CdTe the real misalignment of conduction band is not easily predictable. A work by the group of Darmstadt University reports a small $\Delta E_C \cong 0.03$ eV in real CdS/CdTe structures [4].

In this work CdS is deposited by HVE (high vacuum evaporation), process starts with a pressure in the evaporation chamber lower than 10^{-5} mbar. At first TCO is annealed at 450°C for 30 minutes. Then CdS is deposited at 100°C of the substrate temperature in high vacuum and then annealed at 450°C for 30 minutes in order to ensure better crystalline quality. Typical CdS thickness in this work is 500 nm.

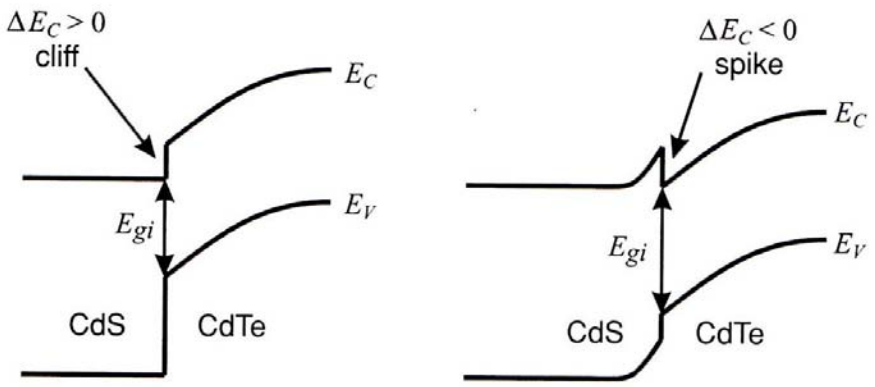

Figure 1.2: Representation of the band diagram alignment at the CdS/CdTe interface.

1.3 CdTe absorber layer

CdTe is the p-type semiconductor of our p-n junction, energy gap reported in literature ranges from 1.4 eV to 1.56 eV. It is a direct bandgap semiconductor, so absorption process doesn't involve phonon like in silicon PV cells. Thanks to these material properties, CdTe has a very high absorption coefficient: 92% of the useful sunlight could be converted with only $1\mu m$ of this material, while $200\mu m$ of crystalline silicon are necessary to reach the same value.

CdTe is deposited in high vacuum at 340°C of substrate temperature and pressure lower than 10^{-5} mbar. Standard thickness values used in this work are 9 μm of CdTe, before activation treatment samples are called as-deposited. Glass substrate dimensions are roughly 3cmX3cmX0.5cm, each substrate is halved before treatment. Each run deposits thin films on 4 glass substrates at the same time so 8 samples per run are made. Treated sample is usually etched (paragraph 1.5) before making back contact, so final device thickness ranges from 7 μm to 7.5 μm.

1.4 $CdCl_2$ activation treatment

CdTe treatment with chlorine is a fundamental step to achieve high efficiencies solar cells. There are many different technique to do this: it is possible to deposit a thin solid film of $CdCl_2$ by evaporation or by CSS, or with a $CdCl_2$ methanol saturated solution bath. Then sample is heated in oven to start the following reaction:

$$CdCl_2(s) + 0_2(g) + CdTe(s) \Longleftrightarrow TeCl_2(g) + 2CdO(s) \tag{1.1}$$

The effects of $CdCl_2$ treatment has multiple effect:

- Grain size increase due to chlorine reaction
- Promotion of CdS/CdTe intermixing layer
- Improved p-type doping in CdTe
- Density of deep electronic states in bulk or at the interface can be reduced and different deep states can be introduced

- Overtreatment can cause a V_{oc} loss due to the introduction of deep recombination centers. It can also cause loss of adhesion of the film.

Typical treatment uses solution with roughly 0.16g of mono-hydrate $CdCl_2$ in 100 ml of methanol[1] (roughly 10% of saturation value). Deposition is made with 40 drops[2] of solution dropped on the as-deposited sample and the methanol is left evaporate under chapel. $CdCl_2$ is removed from front contact area with water using a wet cotton swab. Dried sample is heated in oven in air atmosphere at 410°C with 20 minutes of ramp time and 30 minutes of treatment. Chapter 2 will deeply discuss issues related to this step process.

1.5 Etching and back contact

After activation treatment, samples surface should be cleaned by $CdCl_2$ residue to improve back contact quality. Due to CdTe high electron affinity, high work function of metal is required, many back contacts have been studied and developed (Sb_2Te_3, As_2Te_3, etc.), however best results were achieved with the addition of Cu. Copper compounds such as CuTe, Cu_2Te etc. results in good ohmic contact, on the other hand copper high diffusion tendency cause performance degradation on aged devices.

Treated samples are etched to clean the surface from $CdCl_2$ residue dipping and shaking the sample in a solution bath usually made with 40 ml of methanol and 5 drops of bromine for 40 seconds. Then sample is put in a vacuum evaporation chamber, 2 nm of copper and 50 nm of gold are deposited on the surface at room temperature with pressure lower than 10^{-5} mbar. Copper and gold deposition rate are in the range of 0.01-0.03 nm/sec and 0.1-0.25 nm/sec respectively. Gold is deposited to prevent copper oxidation. We used a molybdenum shadow mask to deposit an array of 10 round holes with 0.13 cm^2 area. Final step is the annealing of back contact in air at 190°C with 15 minutes of ramp time and 20 minutes of annealing.

1.6 Conclusion

The whole process developed at Verona University's laboratories is made at low temperatures (≤ 450°C). CdTe solar cells fabricated in these laboratories exceed 15% efficiency. Each run takes 3-4 days to be accomplished and has 8 as-deposited samples as output. Each sample needs 1-2 days more to make treatment, etching and back contact. More information about the process can be found in [3]. Figure 1.3 and 1.4 show how the sample look like.

[1] Solubility of $CdCl_2$ in water is higher than in methanol but the surface tension avoid solution to spread on the sample, so water is useless for deposition purpose. Handbook of chemistry states that saturation value of $CdCl_2$ in methanol is 1.7g/100ml.

[2] Each drop contains 18 μl of solution.

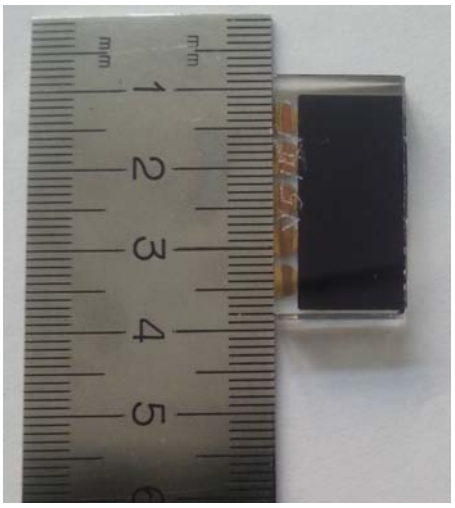

Figure 1.3: This figures show the frontside of the sample where the device is enlightened.

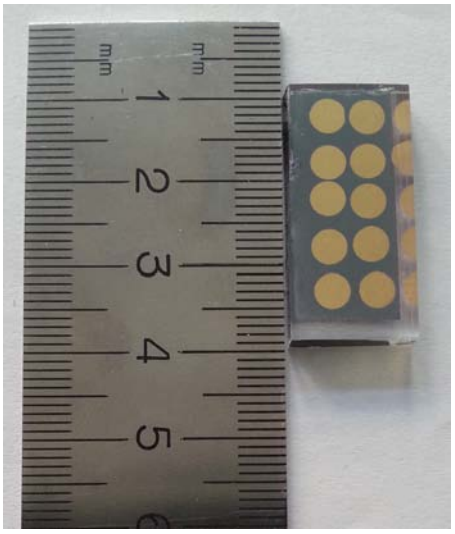

Figure 1.4: This is the backside of the sample. Each circle is a solar cell that works independently from the other. Half circle on the left are the front contact of the cells as they are deposited directly on the TCO. Sample numeration index are [row,column] with front contact on the right. Row increase from up to down, column increase from right to left. In example upper right corner is cell 11 and bottom left corner is cell 52.

Chapter 2

Activation treatment step process

This chapter is focused on $CdCl_2$ activation treatment procedure. We studied how to prepare a stable solution of $CdCl_2$ to have reproducible deposition and devices efficiencies.

2.1 Treatment baseline

Solution called *"satura"* was made with 0.8 g of $CdCl_2$ dissolved in 100 ml methanol corresponding to a concentration of 47% of saturation limit value[1], it was stirred continuosly with a magnetic stirrer. *Satura* solution was diluted: sol. B was made with 20 ml of *satura* solution and 80 ml of methanol, hence sol. B has a concentration of 9.4%.

To simplify this procedure, solution I was directly made with 0.161 g of $CdCl_2$ mono-hydrate in 100 ml of methanol corresponding to 9.47% of saturation limit value, then it was left on the stirrer for three days before using it. In the meanwhile we also prepared solution II with 0.2455 g of the same powder of $CdCl_2$ that means a concentration of 14.4%. Samples were treated as usual (see paragraph 1.4) with 40 drops of solution I or II at 410°C with 20 min of ramp time and 30 min of treatment. Some samples were etched for 5 seconds so the surface recrystallization was still visible after etching and could be checked in the future. As treatment becomes more stable all samples will be etched for 40 seconds to reach higher efficiencies (for more information see [3]).

Devices efficiencies made with these solutions are reported in table 2.1, 2.2 and 2.3. If reported efficiency is S. (shunt), it means that cell is shunted for some reasons related to the process; while if T.S. (technological shunt) is reported, it means that shunt is caused by external problem: e.g. alignment error between sample and back contact shadow mask, bad cut of glass substrate etc. Therefore cells with T.S. are not representative of process quality and should not be taken into account.

We noticed that both samples treated with sol. I dried bad, some border parts dried fast, leaving no $CdCl_2$ on the surface, moreover frontside was ruined after treatment showing small white spot on the CdS side of the cell.

[1]Solubility of $CdCl_2$ in water is higher than in methanol but the surface tension avoid solution to spread on the sample, so water is useless for deposition purpose. Handbook of chemistry states that saturation value of $CdCl_2$ in methanol is 1.7g/100ml.

Sample V4332 treated with solution II exhibited a 13% as best case (table 2.3), so we tried to repeat the treatment with longer etching trying to improve this result. Unfortunately solution started to dry worse leaving empty parts on the surface. V4331 had only 1 working cell out of 8. V4312 worked better but was not so good compared to V4332 or to samples treated with solution B[2].

Solution B			
V4302 Etching:5s		V4281 Etching:5s	
cell	η	cell	η
11	8.2%	11	9.3%
12	10.2%	12	S.
21	7%	21	9.5%
22	7.8%	22	9.3%
31	9.4%	31	9.4%
32	8.7%	32	11.4%
41	9.2%	41	12%
42	2%	42	10.3%
51	12%	51	6.5%
52	11.3%	52	5%

Table 2.1: Efficiencies of samples made with solution B.

Solution I			
V4301 Etching:5s		V4311 Etching:5s	
cell	η	cell	η
11	T.S.	11	7.3%
12	4.8%	12	6.3%
21	T.S.	21	6.1%
22	1.8%	22	6.9%
31	T.S.	31	6.1%
32	0.8%	32	T.S.
41	T.S.	41	3.8%
42	0.5%	42	4.1%
51	T.S.	51	7%
52	1.2%	52	5.4%

Table 2.2: Efficiencies of samples made with solution I.

Solution II					
V4332 Etching:5s		V4331 Etching:40s		V4312 Etching:40s	
cell	η	cell	η	cell	η
11	1.4%	11	T.S.	11	8.7%
12	S.	12	5.9%	12	T.S.
21	7%	21	T.S.	21	S.
22	S.	22	S.	22	5.8%
31	8.6%	31	S.	31	4.6%
32	6%	32	S.	32	3.7%
41	10.8%	41	S.	41	8.3%
42	9.6%	42	S.	42	4.5%
51	10.2%	51	S.	51	8.8%
52	12.9%	52	S.	52	11.7%

Table 2.3: Efficiencies of samples made with solution II.

[2]Solution B used to work better but results worsened as solution age increased.

2.2 Feedback of step process

To stabilize this step process we had to outline some desirable features of the activation treatment.

1. Homogeneous drying
2. Seeds crystals of $CdCl_2$
3. Good recrystallization
4. Perfect frontside
5. High efficiency

Homogeneous drying means homogeneous solution, bad dried samples shows some empty parts where methanol evaporates very fast, this happens because $CdCl_2$ is not well distributed in methanol solution. So this feature is necessary in order to have a uniform distribution of $CdCl_2$ on the sample surface. Sometimes we measured the time needed to deposit a fixed number of drops and the time needed to let the methanol evaporate. The deposition rate of $CdCl_2$ is decided by the operator's feeling, drops are put fast enough to avoid that sample totally dries before all the drops are deposited and slow enough to avoid solution to fall down from the surface; so we didn't expect a fixed time for deposition but we just warned about large differences from usual values.

We took images of $CdCl_2$ morphology and images of recrystallization of CdTe grains size with optical microscope. We also took images with AFM (Atomic Force Microscope) for a better characterization of valuable samples (see chapter 4) but optical microscope gives faster response and it is more useful for an immediate feedback about deposition or treatment; sometimes we didn't waste time finishing samples that dried bad or didn't show any recrystallization after treatment. Figures 2.1-2.6 are useful to understand the description of $CdCl_2$ morphology given in this chapter. Figures 2.7-2.8 show images of CdTe surface after annealing of $CdCl_2$. We thought that seeds crystals would be better because they are more spread over the surface, while small and big crystals, due to a localized concentration of $CdCl_2$, may ruin the frontside. We found that this feature was unnecessary to achieve high efficiencies (see paragraph 2.7).

Another important feedback is the frontside of the cell: from the CdS side as-deposited samples looks totally black, but due to a strong treatment, $CdCl_2$ could penetrate deeper damaging the CdS film (figures 2.9 and 2.10). Small white spot are visible on the frontside in case of too strong intermixing between CdS and CdTe or a loss of adhesion of CdS from the glass substrate. Samples with ruined frontside have low efficiencies.

Finally we measured cells efficiencies to discriminate good and bad treatment. Measurement system will be discussed in chapter 3.

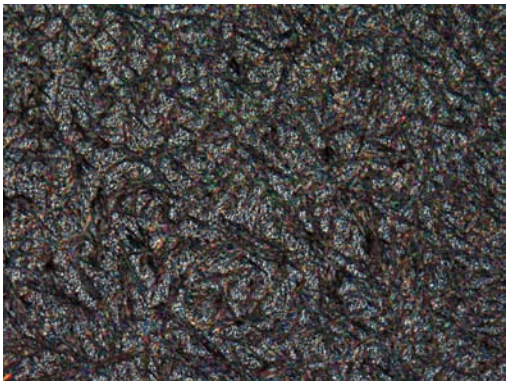

Figure 2.1: Seeds crystals, 5x magnification.

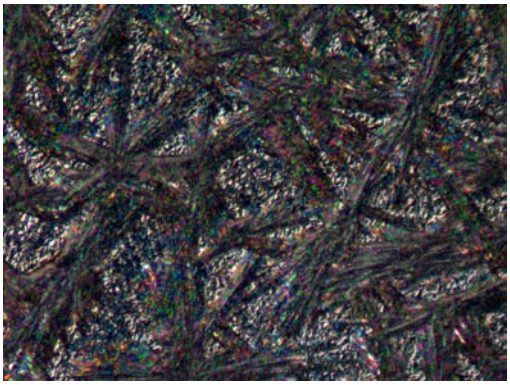

Figure 2.2: Seeds crystals, 50x magnification.

Figure 2.3: Small crystals, 5x magnification.

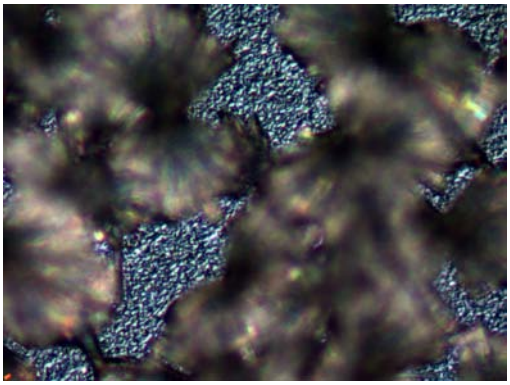

Figure 2.4: Small crystals, 50x magnification.

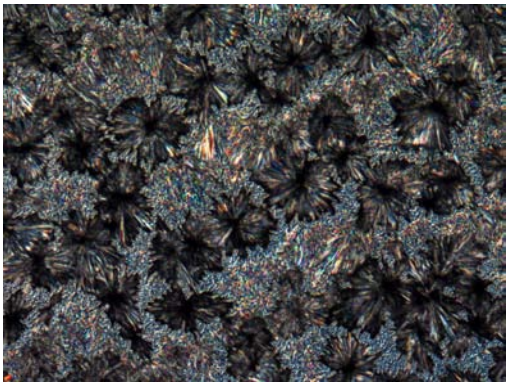

Figure 2.5: Big crystals, 5x magnification.

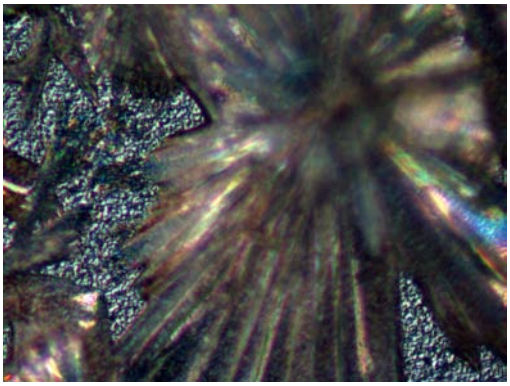

Figure 2.6: Big crystals, 50x magnification.

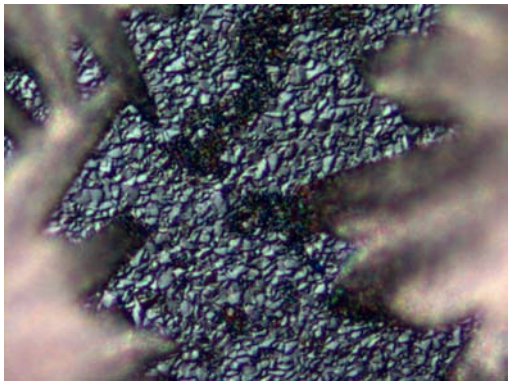

Figure 2.7: Bad recrystallization. CdTe grains size is similar to as deposited samples.

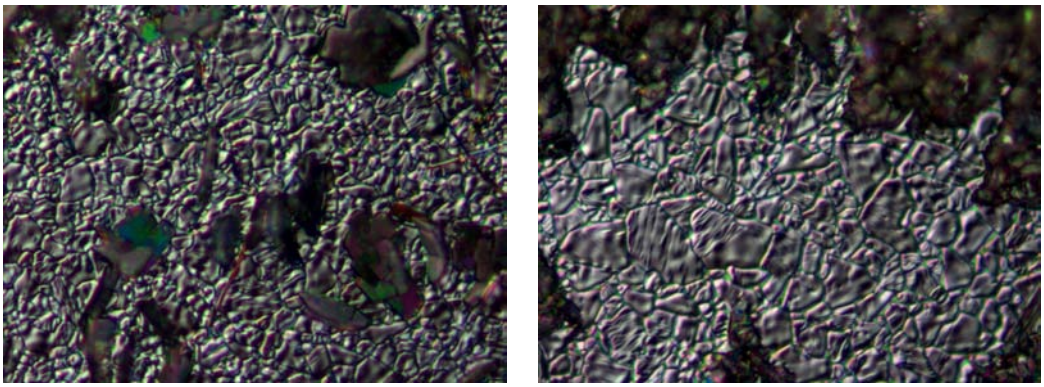

Figure 2.8: Good recrystallization. This step is mostly qualitative. Sample on the right shows bigger grains than sample on the left, but we classify both as good.

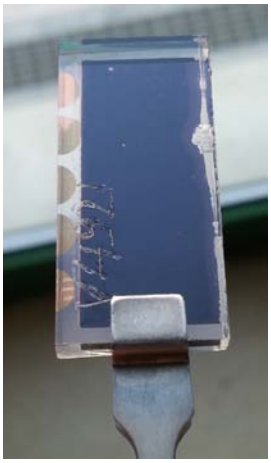

Figure 2.9: Good frontside. Enlightning the sample we can see that sample is almost uniform except the small border on the right.

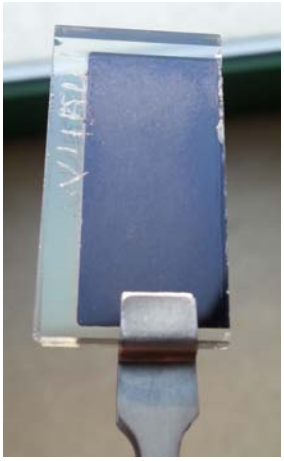

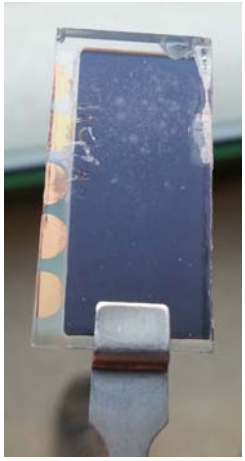

Figure 2.10: Bad frontside. Sample on the left shows wide area where the film becomes brighter. On the right white spot are more localized in the upper part of the sample.

2.3 Heating solution

We made new solutions saturated at 60%, this could speed up $CdCl_2$ deposition but could cause problems of solution homogeneity. Solution IV was made in four steps in 200 ml of methanol, leaving enough time stirring to let $CdCl_2$ dissolve (table 2.4). Solution V was made in a single step putting 1.0177 g of $CdCl_2$ in 100 ml of methanol equal to 59.86%.

Even if sample V4352 dried quite good, it had lots of shunt and low efficiencies, we let solution stirring for few days, we repeated the same treatment on sample V4322 but it worked even worse (see tables 2.5 and 2.6).

We tried to improve the activation treatment heating solution at 50°C for 10 minutes and using it after 30 minutes of cool down. The aim was to verify if heat could reset any changes in solution, dissolving any presence of precipitate in suspension. Sample V4431 was rejected because frontside was heavily damaged.

We also made few samples with sol. V but worked as bad as sol. IV. Heating solution for a long time had slightly better results as shown by sample V4441: efficiencies ranged from 6.5% to 12.1%.

We also tried to use again sol. IV without heating it. V4372 was rejected because of bad drying leaving most of sample empty, V4361 was rejected because CdTe did not recrystallize. We decided to use a solution with less $CdCl_2$ and heat it for a long time before deposition.

	$CdCl_2$ added	concentration	time left stirring
Step I	0.5205g	15.3%	27m
Step II	0.5165g	30.5%	26m
Step III	0.682g	50.5%	18h
Step IV	0.350g	60.8%	1 day

Table 2.4: Making solution IV. All values are referred to 200ml of methanol.

Solution IV					
V4352		V4322		V4441	
cell	η	cell	η	cell	η
11	S.	11	S.	11	T.S.
12	S.	12	S.	12	7.8%
21	3.3%	21	2.3%	21	T.S.
22	7.9	22	S.	22	T.S.
31	S.	31	2.4%	31	7.9%
32	S.%	32	1%	32	6.5%
41	4.9%	41	6.5%	41	10.4%
42	8.4%	42	2.6%	42	9.6%
51	10.6%	51	T.S.	51	11.7%
52	9.7%	52	4.9%	52	12.1%

Table 2.5: Efficiencies of samples made with solution IV.

Sample	**V4352**	**V4322**	**V4431**
Solution temperature	room	room	50°C, few min
Drops	6	6	6
Drying	empty corner	good	good
$CdCl_2$ morphology	N.A.	crystals	crystals
Recrystallization	good	good	good
Frontside	good	bad	bad
Etching	40s	40s	N.A.
η_{max}	10.6%	6.5%	N.A.

Sample	**V4441**	**V4372**	**V4361**
Solution temperature	50°C, long time	room	room
Drops	6	3+6	3
Drying	good	bad	good
$CdCl_2$ morphology	small crystals	big crystals	small crystals
Recrystallization	good	N.A.	bad
Frontside	bad	N.A.	bad
Etching	5s	N.A.	N.A.
η_{max}	12.1%	N.A.	N.A.

Table 2.6: Description of depositions made with solution IV. N.A. means not available.

2.4 Using anhydrous powder of $CdCl_2$

As $CdCl_2$ is highly hygroscopic, powder used to make solution changes his properties and composition. For this reason we decided to heat the powder in high vacuum at 100°C and keep it in vacuum chamber. This step allows to improve reproducibility of our solution, deleting presence of water from $CdCl_2$ powder that is an environmental variable out of control. Table 2.7 represents data obtained from anhydrating $CdCl_2$ powder. We increased chamber temperature with small steps because water evaporation could increase the pressure and deal damage to turbomolecular pump.

Time	Temperature	Pressure	Comments
0 min	28°C	atm	start roughing pump
35 min	28°C	$4.6 \cdot 10^{-2} mbar$	start turbo pump
60min	28°C	$1.4 \cdot 10^{-3} mbar$	pressure is stable, stop turbo
61min	28°C	$3.6 \cdot 10^{-2} mbar$	start heating up to 50$_\circ$C
70min	50°C	$5.3 \cdot 10^{-2} mbar$	set point up to 70°C
86min	70°C	$1.3 \cdot 10^{-1} mbar$	
101min	70°C	$4 \cdot 10^{-1} mbar$	
128min	70°C	$3.5 \cdot 10^{-1} mbar$	set point up to 100°C
145min	100°C	$4.5 \cdot 10^{-1} mbar$	stop temperature (going home)
18h 12min	33°C	$1.7 \cdot 10^{-3} mbar$	set point up to 100°C
19h 00min	100°C	$1.9 \cdot 10^{-3} mbar$	start turbo
19h 05min	100°C	$1.5 \cdot 10^{-4} mbar$	
19h 20min	100°C	$1.2 \cdot 10^{-4} mbar$	stop heating, powder ready
23h 40min	63°C	$7.3 \cdot 10^{-6} mbar$	

Table 2.7: Temperature ramp to anhydrate $CdCl_2$ powder.

Solution VI was the first made with anhydrated powder (30% of saturation value) and was stirred three days before using it. We reduced solution's concentration in order to obtain seeds crystals of $CdCl_2$. With this goal in mind we also reduced to 10 the number of drops of solution VI deposited on sample V4471, we heated the solution and we waited for cooldown[3] before deposition on sample V4472; second sample dried better and showed seeds of $CdCl_2$ on the surface sample, while the other had small crystals on the surface (table 2.9). However treatment at 410°C was not enough effective to recrystallize CdTe grains.

We made two samples with 20 drops: V4882 before heating solution VI, and V4881 after heating; they both dried good with small crystals of $CdCl_2$ on the surface. Sample V4881 exhibited lower efficiencies than V4882 (table 2.8).

Both frontsides were damaged after treatment and we decreased treatment temperature from 410°C to 390°C[4] to see if this would solve the problem, result

[3]Everytime we heated or boiled any solution, we also waited enough time to cool the solution. If we used a warm solution we would have lost information about the real amount of $CdCl_2$ deposited as warm solution has different density.

[4]Ramp time was set to 25 minutes instead of 20, treatment time was set to 30 minutes like in the old treatment.

was good (table 2.10), frontside was clean and we noticed higher V_{oc} for all cells that belonged to sample V4491 compared to other samples made at 410°C.

We tried to get the same result decreasing the number of drops instead of treatment temperature but solution VI started to behave in a strange way. After the deposition first half of both samples V4462 and V4461 dried fast leaving seeds on the surface, while the second half took more time to let the methanol evaporate leaving big crystals on the surface. 15 drops of sol. VI at room temperature were deposited on V4462, while 12 drops were deposited on V4461 after heating solution. Efficiencies are very low for these two samples (table 2.8) and V_{oc} are lower than V4491 for most cells of both samples.

We tried with 10 drops and 30 drops on samples V4492 and V4511, both dried very bad showing big area without $CdCl_2$. Solution resulted unstable and heat had negative effects because after only two weeks deposition results were not reproducible, small empty area could be accepted even if not desirable, but if $CdCl_2$ concentrate in a half of the sample probably solution should be changed with a new one.

In conclusion a lower treatment temperature solved the problem of the frontside, decreasing number of drops was less effective than lowering treatment temperature, treatment was not yet stable but efficiencies were more homogeneous, samples showed less shunt than before probably thanks to anhydrous powder of $CdCl_2$, heating solution does not improve the deposition of $CdCl_2$ as samples with heated and not heated solution dried good or bad in the same way. Is not possible yet to evaluate any advantage by presence of $CdCl_2$ seeds, sample V4491 had a good frontside and quite good efficiency even in presence of small crystals, by the other hand samples V4662 and V4661 showed both seeds and small crystals and higher efficiencies are located in the lower part where seeds crystals were deposited.

Solution VI			
Not heated		Heated	
V4482 20 drops		V4481 20 drops	
cell	η	cell	η
11	6.5%	11	S.
12	6.3%	12	7.1%
21	8%	21	6.9%
22	7.3%	22	6.9%
31	8%	31	6.2%
32	7.2%	32	6.7%
41	7.3%	41	5.1%
42	8.7%	42	S.
51	11.5%	51	7%
52	9.1%	52	8.7%

Solution VI			
Not heated		Heated	
V4462 15 drops		V4461 12 drops	
cell	η	cell	η
11	3.5%	11	3.7%
12	2.4%	12	4.9%
21	S.	21	4.9%
22	2.6%	22	T.S.
31	4.6%	31	4.3%
32	4.3%	32	4.7%
41	7%	41	4.7%
42	6.6%	42	7.5%
51	6.4%	51	10.9%
52	6.1%	52	9%

Table 2.8: Comparison between samples made with solution VI heated and not heated before drops deposition.

Sample	**V4471**	**V4472**	**V4482**
Solution temperature	room	50°C, 30 min	room
Drops	10	10	20
Drying	empty corner	good	good
$CdCl_2$ crystals	small	seeds	small
Recrystallization	bad	bad	good
Etching	40s	40s	N.A.
η_{max}	N.A.	N.A.	11.5%

Sample	**V4481**	**V4491***	**V4462**
Solution temperature	50°C, 30 min	room	room
Drops	20	20	15
Drying	not bad	not bad	not bad
$CdCl_2$ crystals	small	small	seeds & small
Recrystallization	not bad	not bad	not bad
Etching	5s	5s	5s
η_{max}	8.7%	11%	6.6%

Sample	**V4461**	**V4492**	**V4511**
Solution temperature	50°C, 30 min	50°C, 30 min	50°C, 30 min
Drops	12	10	30
Drying	not bad	very bad	very bad
$CdCl_2$ crystals	seeds & small	big empty	big empty
Recrystallization	good	N.A.	N.A.
Etching	5s	N.A.	N.A.
η_{max}	10.9%	N.A.	N.A.

Table 2.9: Description of depositions made with solution VI. N.A. means not available.
* This sample was treated at 390°C instead of 410°C.

Solution VI											
V4491				V4482		V4481		V4462		V4461	
cell	η	cell	V_{oc}	cell	V_{oc}	cell	V_{oc}	cell	V_{oc}	cell	V_{oc}
11	8.2%	11	845mV	11	753mV	11	S.	11	641mV	11	634mV
12	T.S.	12	T.S.	12	718mV	12	732mV	12	627mV	12	655mV
21	T.S.	21	T.S.	21	774mV	21	746mV	21	S.	21	676mV
22	10%	22	838mV	22	746mV	22	732mV	22	620mV	22	T.S.
31	T.S.	31	T.S.	31	775mV	31	732mV	31	704mV	31	683mV
32	11%	32	852mV	32	753mV	32	718mV	32	655mV	32	739mV
41	T.S.	41	T.S.	41	746mV	41	725mV	41	810mV	41	753mV
42	10.3%	42	852mV	42	753mV	42	S.	42	767mV	42	788mV
51	T.S.	51	T.S.	51	824mV	51	739mV	51	852mV	51	845mV
52	6.8%	52	852mV	52	796mV	52	774mV	52	845mV	52	831mV

Table 2.10: Comparison between V_{oc} of samples made with high treatment temperature and lower temperature.

2.5 Boiling solution

Solution VIII was made with 0.5226g/100ml (30.7%) and was left on the stirrer for one day. Then we splitted this solution in two equal parts: sol. VIII_A and sol. VIII_B with the same concentration. We tested if boiling solution could be a viable way to have a repeatable good drying of our samples, we measured how much time it took to let the methanol evaporate; we left sol. VIII_B without stirring while using sol. VIII_A just to verify the importance of stirring.

We boiled sol. VIII_A before deposition on sample V4531. $CdCl_2$ distribution was quite homogeneous with small crystals, time required for sample to dry was 17 minutes, roughly the same time of previous samples[5], it was treated at 390°C and etched for 5 seconds. Sample worked very good, (see table 2.11), no shunted cells, efficiency ranged from 11.3% and 13%. We decided to repeat this result with 40 s etching to improve final efficiency.

V4532 was made without boiling sol. VIII_A before using it and sample dried bad with empty corners and slowly, it took around one hour. Probably solution started to change after being boiled the first time. Treatment temperature was increased to 395°C and sample was etched for 40s. Efficiencies were high showing 3 cells over 13%.

As sample dried very slowly we tried to restore intial conditions by boiling again sol. VIII_A, then we deposited 30 drops on sample V4592. However half sample dried bad with big empty parts, it took half an hour to dry it completely, deposition left big crystals on the surface. Final device had many shunted cells but working cells showed good efficiencies.

We used sol. VIII_B after 10 days without stirring and we tried it on V3901[6], it was a sample with thin CdS, efficiencies were not comparable with normal samples

[5]Drying time of samples made with solution VI discussed in the previous paragraph ranged from 5 to 17 depending on the number of drops.

[6]Due to 100nm of CdS, this sample has higher current. Shunted cells is a drawback of thin CdS and it is not related to $CdCl_2$ treatment. Efficiencies are not comparable with other samples.

but the aim was just to check how the sample would dry: it took one hour, we expected this bad result as solution was not stirred, next attempt was to check if boiling solution could reverse this solution to homogeneity, see table 2.13.

As sample V4501 took 90 minutes to dry we can conclude that heating at high temperature has bad consequences, boiled solutions got worse and took a lot more time to dry, final efficiencies were quite good, but strong evaporation occurs each time we boiled the solution, this may cause strong changes in solution concentration, also quantity of solution decrease very fast after a couple of treatment. Both V4501 and V3901 were treated at 400°C, however frontside looked a little bit spoiled at this temperature. So we decide to keep 395°C as the best treatment temperature.

We stirred sol. VIII_B for three days and made sample V4562 but solution was already spoiled by previous heating. Efficiencies were not so high and ranged from 4.8% to 10.2%. Last try was to let the sample dry while heated to induce a more homogeneous evaporation and so a more homogeneous deposition. Sample VFTO3581[7] took only 10 minutes to dry, it was much better than previous samples.

In conclusion we have no improvement by boiling solutions before deposition, it may work once or twice but solution rapidly finishes due to evaporation and drying time becomes equal to a not stirred solution that surely is not homogeneous. However heating the samples seems to be useful to improve homogeneity of $CdCl_2$ deposition.

Sample	**V4531**	**V4532**	**V4502**
Boiling solution	6 min, cooled	not boiled	2 min, cooled
Drops	40	40	30
Drying	good	not homogeneous	not homogeneous
Drying time	17 min	60 min	30 min
$\boldsymbol{CdCl_2}$ **morphology**	crystals	big crystals	big crystals
Treatment	390°C	395°C	395°C
Recrystallization	good	good	good
Etching	5s	40s	40s
Frontside	perfect	perfect	perfect
$\boldsymbol{\eta_{max}}$	13%	13.5%	13%

Table 2.11: Description of depositions made with solution VIII_A.

[7]This sample has a stack of FTO (fluorine doped tin oxide instead of ITO. Efficiencies are not comparable and it is used only to check the drying time.)

Solution VIII_A					
V4531		V4532		V4502	
cell	η	cell	η	cell	η
11	11.5%	11	12.4%	11	T.S.
12	12.8%	12	12.9%	12	S.
21	11.7%	21	11.8%	21	S.
22	13%	22	T.S.	22	S.
31	12.1%	31	13.5%	31	S.
32	11.8%	32	S.	32	10%
41	12.5%	41	13.1%	41	13%
42	11.3%	42	8.7%	42	8.9%
51	12.8%	51	13%	51	12.3%
52	11.5%	52	11.4%	52	13%

Table 2.12: Efficiencies of samples made with sol. VIII_A.

Sample	**V3901***	**V4501**	**V4562**	**VFTO3581$^+$**
Stirred	no	no	yes	yes
Boiling solution	no	6min, cooled	no	no
Drops	40	40	30	30
Drying	good	empty corner	empty corner	heated, good
Drying time	60 min	90 min	90 min	10 min
$CdCl_2$ crystals	big & small	big	big	big
Treatment	400°C	400°C	395°C	395°C
Recrystallization	good	good	good	good
Frontside	few spots	few spots	perfect	perfect
η_{max}	12.6%	11.6%	12.4%	11%

Table 2.13: Description of depositions made with solution VIII_B. *This sample was made with thin CdS. $^+$This sample was made with FTO as front contact.

Solution VIII_B					
V3901*		V4501		V4562	
cell	η	cell	η	cell	η
11	T.S.	11	10.5%	11	4.8%
12	T.S.	12	10.4%	12	7.7%
21	12.6%	21	10%	21	9.9%
22	8.3%	22	7.2%	22	9.4%
31	S.	31	9.7%	31	7.3%
32	6.1%	32	8%	32	10.5%
41	S.	41	10.7%	41	12.4%
42	S.	42	T.S.	42	8.2%
51	9.3%	51	11.6%	51	T.S.
52	S.	52	7.9%	52	10.2%

Table 2.14: Efficiencies of samples made with sol. VIII_B. *This sample was made with thin CdS.

2.6 Heating samples to obtain a uniform deposition

We made sol. IX with 0.5180g/100ml of anhydrate $CdCl_2$ in methanol (30.47% of saturation value). We decided to avoid heating solution and just let the solution stirring, after few depositions we started to heat samples because solution started to leave small empty parts. Heat induced a uniform evaporation of methanol distributing $CdCl_2$ homogeneously over the sample surface. We made a lot of samples to study the effect of different temperature on the recrystallization of CdTe analyzing both physical and electrical properties of finished devices (see chapter 4). In this paragraph we just report standard check samples made from time to time to verify reproducibility of the activation treatment.

Sample V4561 was made after 1 day of stirring with 40 drops at 395°C (table 2.15). It dried quite good and slightly slow. Efficiencies were high and ranged from 10.2% to 13.4% except for one cell at 4% (table 2.16).

Sample V4551 was made at solution day 6 with same treatment as the previous one but was etched for 5s. Homogeneity was surely good and longer etching would have probably provided better performance.

As V4551 dried a little bit slowly, we heated sample V4571 to obtain a better deposition. We had 14.6% on one cell but lots of shunt: surface showed lots of pinholes through CdS and CdTe films. It could be a problem during deposition of CdS/CdTe stack or a consequence of the activation treatment. Probably first hypothesis was correct as other as-deposited samples of the same run showed some pinholes.

We made two samples in parallel at day 9 to observe the effect of heating the sample. V4592 dried much better than V4591 (table 2.16) and efficiencies were slightly higher so we defined check treatment as: 40 drops of sol. IX, sample dried at 55°C, treated at 395°C with 25 minutes of ramp time and 30 minutes of treatment time, 40 seconds of etching and typical back contact. We also decided to rest solution for a while just before deposition to let fall down any particles in suspension.

Next samples reported in table 2.15 and table 2.16 were all similar, they all had at least one cell at 14% or more, few shunts and all working cells with efficiency higher than 10%. V4702 is the best sample, without shunts and all efficiencies higher than 14%. Best case reached 14.8% efficiency.

Sample	**V4561**	**V4551***	**V4571**
Solution age	1 day	6 days	7 days
Solution rested	no	no	no
Drops	40	40	40
Sample heated	no	no	55°C
Drying time	25 min	35min	5 min
Drying	good, empty corner	upper part empty	good
$CdCl_2$ crystals	small and big	small and big	small
Treatment	395°C	395°C	395°C
Recrystallization	good	good	good
Frontside	perfect	quite good	perfect
Etching	40s	5s	40s
η_{max}	13.2 %	13%	14.6%

Sample	**V4591**	**V4592**	**V4722**
Solution age	9 days	9 days	70 days
Solution rested	no	no	10m
Drops	40	40	40
Sample heated	no	55°C	55°C
Drying time	25 min	9 min	7 min
Drying	upper part empty	good	good
$CdCl_2$ crystals	small & seeds	small	small
Treatment	395°C	395°C	395°C
Recrystallization	good	good	good
Frontside	perfect	perfect	perfect
Etching	40s	40s	40s
η_{max}	13.9%	14%	14.2%

Sample	**4702**	**V4892**	**V4911**
Solution age	89 days	103 days	146 days
Solution rested	10 min	40 min	40 min
Drops	40	40	40
Sample heated	55°C	55°C	55°C
Drying time	1 min	3 min	8 min
Drying	good and fast	good	good
$CdCl_2$ crystals	small	small	small
Treatment	395°C	395°C	395°C
Recrystallization	good	good	good
Frontside	perfect	perfect	perfect
Etching	40s	40s	40s
η_{max}	14.8%	14.6%	14%

Table 2.15: Description of depositions made with solution IX. All samples are treated in oven at 395°C with 25 minutes of ramp time and 30 minute of treatment time. *This sample was etched for 5s because was necessary to other purposes.

Solution IX					
Age: 1 day		Age: 6 days		Age: 7 days	
V4561		V4551		V4571	
cell	η	cell	η	cell	η
11	11%	11	9.2%	11	10.2%
12	13.2%	12	13%	12	S.
21	12.6%	21	11.1%	21	12.2%
22	4%	22	12.1%	22	S.
31	12.1%	31	11.2%	31	S.
32	10.2%	32	12%	32	10.7%
41	12.3%	41	11.3%	41	12.1%
42	12.7%	42	12%	42	S.
51	12.6%	51	11.4%	51	14.6%
52	13.4%	52	11.4%	52	S.

Solution IX					
Age: 9 days		Age: 9 days		Age: 70 days	
V4591		V4592		V4722	
cell	η	cell	η	cell	η
11	10.2%	11	13.2%	11	13.1%
12	12.5%	12	12.6%	12	13.2%
21	9.9%	21	11.9%	21	14.3%
22	S.	22	11.9%	22	11.1%
31	S.	31	S.	31	12.7%
32	9%	32	S.	32	S.
41	S.	41	12.5%	41	13.1%
42	13.9%	42	13.7%	42	10%
51	12.8%	51	14%	51	S.
52	13.2%	52	13.7%	52	11%

Solution IX					
Age: 89 days		Age: 103 days		Age: 146 days	
V4702		V4892		V4911	
cell	η	cell	η	cell	η
11	14.8%	11	12.6%	11	13%
12	14.7%	12	14.5%	12	S.
21	14.1%	21	S.	21	12.1%
22	14%	22	14.3%	22	11.2%
31	14.4%	31	14.6%	31	14%
32	14.2%	32	S.	32	13.9%
41	14.5 %	41	12.6%	41	10.8%
42	14%	42	14%	42	13.6%
51	14.4%	51	14.6%	51	12.2%
52	14.1%	52	14%	52	11.9%

Table 2.16: Efficiencies of check samples made with sol. IX.

2.7 Conclusion

The aim of this chapter was to determine a procedure in order to have a reproducible activation treatment, that means homogeneous and stable solution, uniform distribution of $CdCl_2$ on the surface sample and good recrystallization of CdTe after treatment in oven.

Procedure:

1. $CdCl_2$ must be anhydrated each time before making a new solution
2. Solution must be stirred all the time, and needs about two weeks to work properly
3. Solution must rest for 10-30 minutes just before the deposition of $CdCl_2$
4. Sample must be heated at 55°C after drops deposition to obtain a uniform drying of the surface sample.

Samples made with solution IX followed this procedure and gave good results for 5 months. Samples treated with 40 drops at 395°C usually showed some cells at more than 14% efficiency. Solution age improves samples homogeneity but we must underline that homogeneity is not only related to activation treatment step process, but is also influenced by the whole process from the beginning to the end; especially pin holes on the as-deposited films or a bad cut of sample may cause lack of homogeneity.

Desirable features outlined at the beginning (section 2.2) are all important except number two: we reached high efficiencies without seeds crystals. These results were confirmed by solution XI that was made with the same amount of $CdCl_2$ (0.5116g/100ml, 30% of saturated solution).

Chapter 3

Characterization Techniques

Verified that solution IX was stable and treatment was reproducible, we studied the effect of different temperature over the $CdCl_2$ reaction with the CdS/CdTe junction. We analyzed both physical transformation, through AFM imaging, XRD, Nelson Taylor plot and electrical properties through J-V, C-V, DLCP and QE. This chapter explains in general these measurements and the information that can be obtained.

3.1 Current-Voltage

A p-n junction in dark conditions is a diode which has the property of rectifying electric signals and is characterized by the following equation:

$$J_D = J_0 \left[exp\left(\frac{qV_a}{AkT}\right) - 1 \right] \tag{3.1}$$

J_0 is the saturation current of the diode, A is the ideality factor, V_a is the applied voltage, q is the elementary charge, k the Boltzmann's constant and T the junction working temperature. On light conditions we can model a solar cell as a current generator with a diode in parallel, a shunting resistance R_{sh} and a series resistance R_s see figure 3.1.

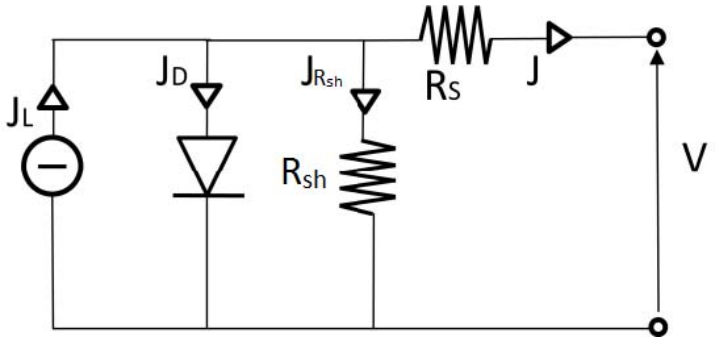

Figure 3.1: Model of a solar cell.

Hence the current J can be calculated as:

$$J = J_L - J_0 \left[exp\left(\frac{q(V - R_s J)}{AkT} - 1\right) \right] - \frac{(V - R_s J)}{R_{sh}} \tag{3.2}$$

J_L also known as short circuit current J_{sc} can be measured in short circuit condition. Without any load connected we can measure the open circuit voltage V_{oc} which can be determined by the following formula:

$$V_{oc} = \frac{kT}{q} ln \left(\frac{J_L}{J_0} - 1 \right) \tag{3.3}$$

A passive load connected at the output terminal should be optimized to set device working point near the maximum power point P_m. Another important parameter for solar cell is called fill factor and it is defined as:

$$FF = \frac{P_m}{V_{oc} J_{sc}} = \frac{V_m J_m}{V_{oc} J_{sc}} \tag{3.4}$$

In ideal conditions, without R_s and R_{sh}, we have $V_m = V_{ov}$ and $J_m = J_{sc}$ hence fill factor would be equal to 1. Finally from previous parameters we can define the efficiency η of a solar cell that evaluate the capability of the device to turn optical power into electrical power:

$$\eta = \frac{P_{el}}{P_{opt}} = FF \frac{V_{oc} J_{sc}}{P_{opt}} \tag{3.5}$$

We used a Keitheley 2420 to measure current-voltage characteristics controlled by a specific ad hoc LabView routine which also encloses to measurement data all parameters used for the entire process [2]. We can use a PT_{100} stuck on the sample surface with a thermal conductive glue to check the working temperature point and keep it controlled by a fan. Light conditions are provided by a calibrated halogen lamp that reproduces an optical power of 1000W/m^2 (standard AM 1.5). Lamp has been calibrated by measuring our cells with a PASAN solar simulator and reproducing cells parameters using the halogen lamp. For daily calibration the current of a silicon photdiode is taken as reference. Applied voltage sweep usually ranges from -0.4V and 1V, it is wide enough to extract all information such as η, FF, V_{oc}, J_{sc}, roll over without damaging our samples.

3.2 Atomic Force Microscopy

Atomic Force Microscopy (AFM) imaging can reach very high resolution of the order of fractions of nanometer. A sharp tip with a radius of curvature of the order of nanometers is located at the end of the cantilever, which is a small beam with dimensions of the order of micrometers usually made in silicon or silicon nitride. The cantilever is characterized by a spring constant k depending on his thickness and length. From this parameter we can define the force and the resonance frequency of the cantilever as:

$$f_{res} = \frac{1}{2\pi}\sqrt{\frac{k}{M}} \tag{3.6}$$

$$F = -k \cdot s \tag{3.7}$$

where M is the mass and s is the deflection of the cantilever. A wide range of cantilevers is commercially available with spring constant ranging from $0.005\frac{N}{m}$ to $40\frac{N}{m}$ to satisfy different purposes.

A laser spot reflected by the head of the tip into an array of photodetectors is used to measure interaction between the tip and the sample surface. Moreover electronic control is required to control many issue of the measurement: processing of photodetectors transduced signals, feedback control to avoid collision between the tip and the sample, regulation of piezoelectric actuators used to scan the sample in x, y, z directions (see figure 3.2).

Interaction between the tip and the sample surface can be described with the van der Waals forces. As a consequence of the zero-point energy, weak force can act between a pair of neutral atoms due to instantaneous dipole induced by quantum effect and the corresponding induced dipole. Attractive potential can be described as $V_{att} = -\frac{B}{r^6}$ while repulsive forces caused by superposition of atomic orbital can be modeled with $V_{rep} = \frac{A}{r^{12}}$. Hence the interaction between the tip and the sample can be described by the Lennard-Jones potential:

$$V_{LJ} = \frac{A}{r^{12}} - \frac{B}{r^6} \tag{3.8}$$

AFM can work in three different mode according to the motion of the tip:

- Contact mode. The tip is dragged across the surface at a depth where the overall force is repulsive, hence this mode is in firm contact with the surface and it is viable only for hard surfaces.

- Non-contact mode. The oscillation frequency of the cantilever is modified by interaction between the tip and the sample surface. Comparing forces near and far from the sample surface is it possible to construct the topographic image of the surface. This method is useful for soft samples as the tip never touches the sample. However it has lower lateral resolution than contact mode.

- Tapping mode. The cantilever vibrate at his resonance frequency, with a higher oscillation amplitude than a non-contact mode. Feedback control acts

in z axis to keep the sample surface at a fixed distance. Hence the information of the surface morphology is extracted by amplitude variation during the scan. It has higher lateral resolution than non-contact mode and does less damage than the contact mode. It can also be used in liquid.

Photodiodes shot noise limits the minimum deflection angle that can be detected, so it limits the resolution of AFM. However this issue is solved by the optical laser power. A 1mW laser is usually enough to achieve 70db of SNR. Another problem is that temperature interact with the tip motion hence thermal noise should be negligible compared to forces induced by the surface sample. This problem can be solved choosing a tip with a proper spring constant:

$$\left\langle \frac{1}{2}(\Delta z)^2 \right\rangle \approx \frac{1}{2}k_B T \tag{3.9}$$

where $k_B T = 4 \cdot 10^{-21} J$ at room temperature and Δz is the vertical resolution in z axis. Choosing a cantilever with $k = 1\frac{N}{m}$ we obtain $\Delta z = 0.5nm$. The main problem that affects AFM resolution is the radius of curvature of the edge of the tip so it is related to technical capability of tip production. Currently resolution of the order of angstrom is possible only for plain surfaces but tips improvement may extends high resolution to rough samples.

Images of CdTe morphology are obtained using AFM in tapping mode. It is not required any particular preparation of the sample before the scan, finished device is etched for 40 seconds with 5 drops of bromine in 40 ml to clean the surface and put under the tip. Instrumentation set up requires some time as the laser has to be centered on the tip and photodiodes must be aligned with the reflection of the cantilever. Moreover surface scans need a lot of time.

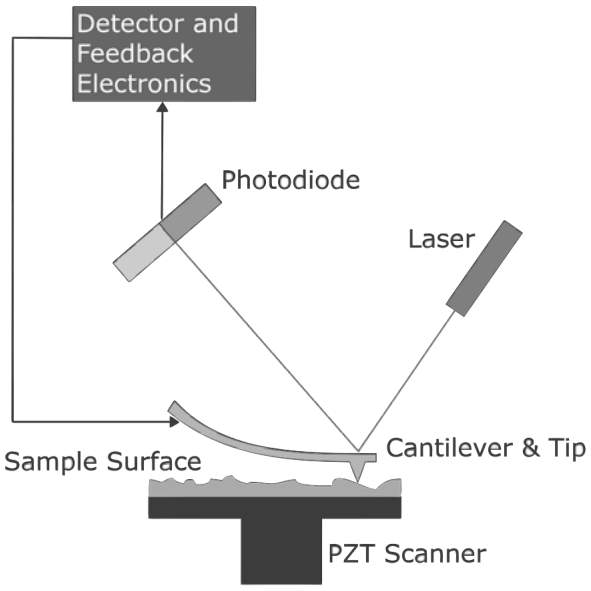

Figure 3.2: AFM blockdiagram. Cantilever deflection are detected measuring the reflection of the laser beam with an array of photodiodes. Electronic devices control sample movement through piezoelectric actuators.

3.3 X-Ray Diffraction - Nelson Taylor Plot

X-rays incident on an atom interact with the electronic cloud causing charge movement that re-radiates waves with the same wavelength of the incident beam, this is also known as Rayleigh scattering. Applying X-rays on a crystalline solid, each atom re-emits a wave at the same frequency of the incident one but with different phases, hence a diffraction pattern can be observed due constructive and destructive interference between scattered waves. Considering an interplanar distance d between lattice planes (figure 3.3) and two beams with a scattering angle θ, the difference path can be calculated as $2dsin\theta$. Bragg's law states that for constructive interference the difference path must be a multiple of the wavelength:

$$2dsin\theta = n\lambda \tag{3.10}$$

Bragg peaks of the diffraction pattern allows identification of the composition of the sample. Defining a the lattice spacing for a cubic crystal we can calculate a as:

$$a = \frac{\lambda}{2} \cdot \frac{\sqrt{h^2 + k^2 + l^2}}{sin\theta} \tag{3.11}$$

where h,k,l are the miller indices of the Bragg plane and λ the radiation wavelength.

Nelson-Taylor plot allows to extract the true unit cell dimension by using a function of the Bragg angle θ and the values of the lattice spacing. It may be shown that absorption error in the apparent unit cell dimension a is linear against a function of θ [7]:

$$\frac{\delta a}{a} \propto \frac{1}{2} \cdot \left(\frac{cos^2\theta}{sin\theta} + \frac{cos^2\theta}{\theta} \right) \tag{3.12}$$

And the error tends to zero approaching $\theta = 90°$. Practically lattice parameter is calculated as the intercept of the plot of a values (obtained from different crystallographic planes) against $f(\theta)$ shown in equation 3.12.

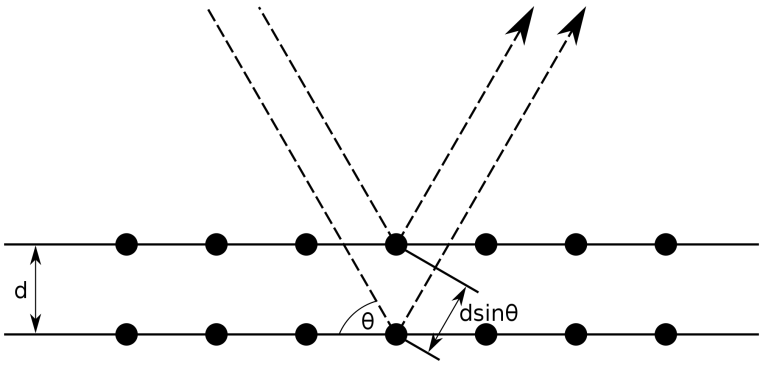

Figure 3.3: Different path between two waves scattered by successive crystallographic planes.

In our case we used the diffraction pattern to reveal transformation of crystallographic preferred orientation induced by $CdCl_2$ activation treatment on post growth CdTe thin film.

X-ray diffractometer is used to detect the diffraction pattern of the sample by measuring the intensity of the scattered waves as a function of the Bragg angle.

X-ray tube is kept in vacuum and power supply is set at 40kV and 2.5mA. By thermoionic emission the hot cathode emit an electron, which is accelerated by the electric field between anode and cathode (see figure 3.4). Anode is made by a target material, in our case by copper. When the electron emitted by the hot cathode hits the target usually it has enough energy to knock an orbital electron out of the inner electron shell of the target atom. As a consequence of the electrons relaxation from higher energy levels to fill up the vacancy, X-ray photons are emitted through a beryllium window. Copper anode emission is called $K_{\alpha 1}$ which has $\lambda = 0.154nm$ and is the reference X-ray used in this work, also K_{β} radiation is emitted but with lower intensity. Finally a divergence slit is used to focus the emitted X-rays, this allows to change the spot area of the sample irradiated by X-rays.

The receiving part of the instrument is made by a peltier detector, silicon doped with lithium, with a slit used to focus detector eye on the radiation emitted by the sample. Both emitter and receiver need an efficient system of cooldown to safeguard integrity of the components. Emitter and receiver have a synchronous movement while performing the measurement called Bragg-Brentano theta theta configuration. The angle between the incident beam and the sample is always equal to the angle between the reflected beam and the sample during the scan. Diffraction pattern of samples reported in the next chapter are kindly provided by Professor Fabio Piccinelli, department of Biotechnology, University of Verona.

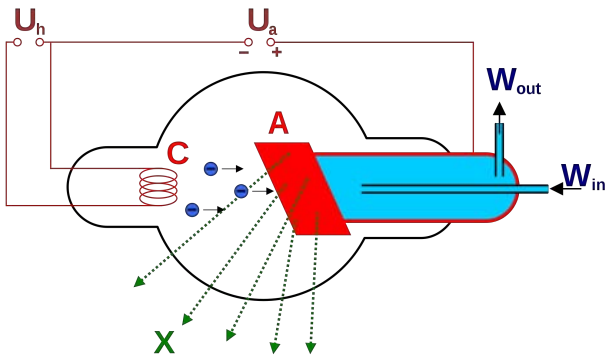

Figure 3.4: Model of a X-ray emitter tube.

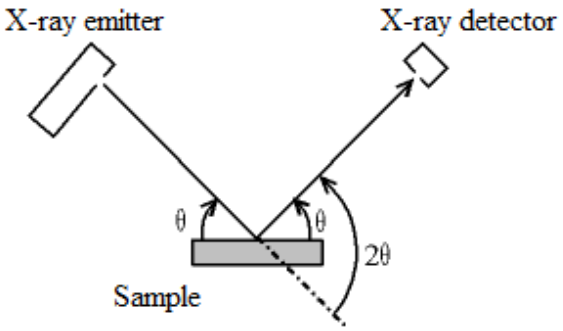

Figure 3.5: Representation of the Bragg-Brentano theta theta configuration.

3.4 Capacitance-Voltage and Drive Level Capacitance Profile

This paragraph describes the Capacitance-Voltage (CV) and the Drive Level Capacitance Profiling (DLCP) techniques. Both provide informations about the density of defect states within the bandgap of the semiconductor and are used to estimate the net free carrier density in the film[2][5].

3.4.1 Approximation and assumptions

To perform these measurement a superposition of a direct current voltage V_{DC} and an alternate current voltage V_{ac} is applied to the sample measuring the output current J. Solar cell can be modeled as a capacitance with a parallel resistance, figure 3.6 shows a model for the setup measure.

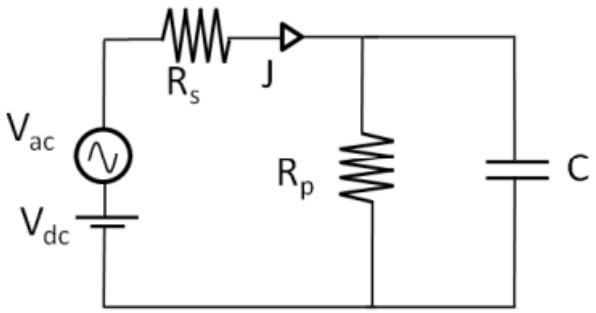

Figure 3.6: Solar cell equivalent circuit for admittance measurements.

Admittance Y is defined as

$$Y = \frac{J}{V_{DC} + V_{ac}} = G + jB \tag{3.13}$$

and

$$C = \frac{B}{\omega_{ac}} \qquad and \qquad \omega_{ac} = 2\pi f_{ac} \tag{3.14}$$

where f_{ac} is the frequency of the small signal V_{ac}. The conductance G of our model should be small to have a reliable estimation of the capacitance C.
The quality factor Q defined as:

$$Q = \frac{|Im(Y)|}{Re(Y)} = \frac{|B|}{G} = tan\left(\frac{\pi}{2} - \varphi\right) \tag{3.15}$$

would be ideally ∞ for a pure capacitance. For this type of measures $\varphi > 80°$ (see figure 3.7) is necessary to consider negligible measurement error.

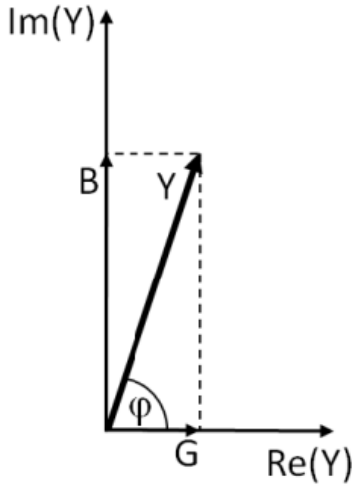

Figure 3.7: Admittance representation in phasor diagram.

We assume in the model of p-n junction that:

- SCR is fully depleted of free carriers
- SCR ends abruptly
- SCR is precisely defined
- SCR extends only in CdTe layer as CdS is considered highly doped compared to CdTe

3.4.2 C-V

Solar cell can be considered as a capacitor where the depletion region work as an insulator and the neutral regions are the conductors plates. Capacitance value of this system can be calculated as:

$$C = \frac{Q}{V} = \frac{\epsilon_r \epsilon_0 A}{W} \tag{3.16}$$

where Q is the electrical charge of the SCR, ϵ_r the dielectric constant of the material, A the area of the device, W the depletion region width. Moreover capacitance are measured applying small signal variation as:

$$C = \frac{dQ}{dV} \tag{3.17}$$

As stated in the previous paragraph, extension of the space charge region in CdS is negligible and the depletion region width can be ideally calculated as:

$$W = \sqrt{\frac{2\epsilon_r \epsilon_0 (V_{BI} - V_{DC})}{qN_A}} \tag{3.18}$$

where V_{BI} is the built in voltage, and N_A is the acceptor state density.

Hence substituting 3.18 in 3.16 we can calculate:

$$C^2 = \frac{\epsilon_r^2 \epsilon_0^2 A^2}{W^2} \qquad \Rightarrow \qquad \frac{1}{C^2} = \frac{2}{A^2 q N_A \epsilon_r \epsilon_0}(V_{BI} - V_{DC})$$

differentiating by our control variable V_{DC}

$$\Rightarrow \qquad \frac{d(1/C^2)}{dV_{DC}} = -\frac{2}{A^2 q N_A \epsilon_r \epsilon_0} \qquad \Rightarrow \qquad \boxed{N_A(W) = -\frac{2}{A^2 q \epsilon_r \epsilon_0}\left(\frac{d(1/C^2)}{dV_{DC}}\right)^{-1}} \tag{3.19}$$

Equation 3.19 shows that we have a relationship between the device capacitance and the charge density of the depletion region at the edge of the SCR. Practically we need a superposition of a small signal (typically 50mV) over the sweep of V_{DC} to measure the capacitance voltage characteristic. Hence we can estimate the depletion region width corresponding to applied V_{DC} voltage and plot the acceptor density profile over the distance from junction.

Nevertheless $N_A(W)$ extracted with this technique, overestimate the value of the shallow dopant in presence of significant deep states, that is our case for CdS/CdTe solar cells. Indeed the small signal v_{ac} applied, causes small variations of the band bending and as a consequence, deep defects states densities may change their cross point with the fermi level E_F, see figure 3.8. Temperature and small signal frequency f_{ac} can change the effect of defect contribution.

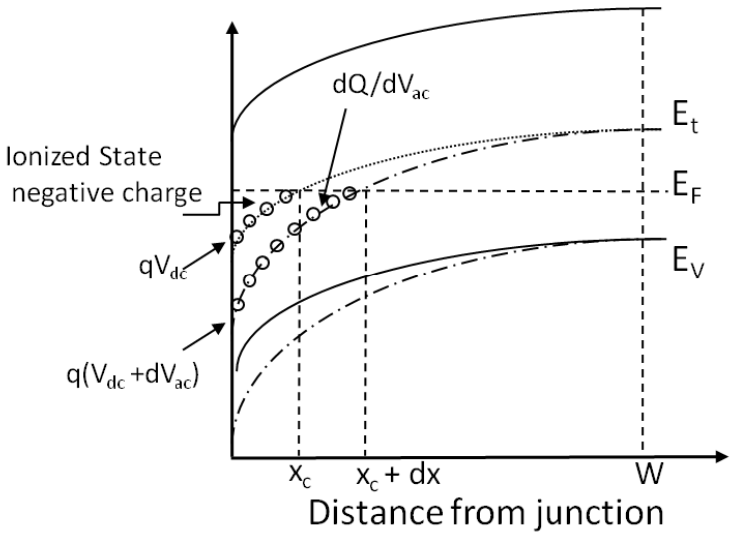

Figure 3.8: Deep defect response to applied V_{ac}.

3.4.3 DLCP

Equation 3.17 is true for ideal capacitance, however in real devices second order effects leads to a nonlinear response to larger amplitudes of the applied V_{ac} .

$$\frac{dQ}{dV} = C_0 + C_1 dV + C_2 (dV)^2 + \ldots \tag{3.20}$$

Higher order terms in equation 3.20 are used in DLCP technique to deduce more accurately the value of the shallow defects in our semiconductor bandgap. As the frequency of the small signal applied and the temperature of the measurement change the response of a defect, we define the limiting energy E_e as follow:

$$E_e = -kTln\left(\frac{\omega_{ac}}{2\pi v_0 T^2}\right) \tag{3.21}$$

where $v = v_0 T^2 = N_v(T)\langle v\rangle\sigma_h$ is the thermal emission prefactor and takes into account the effective density of states in the valence band N_v, the average thermal velocity $\langle v\rangle$ and the capture cross section σ_h of the state involved[1].

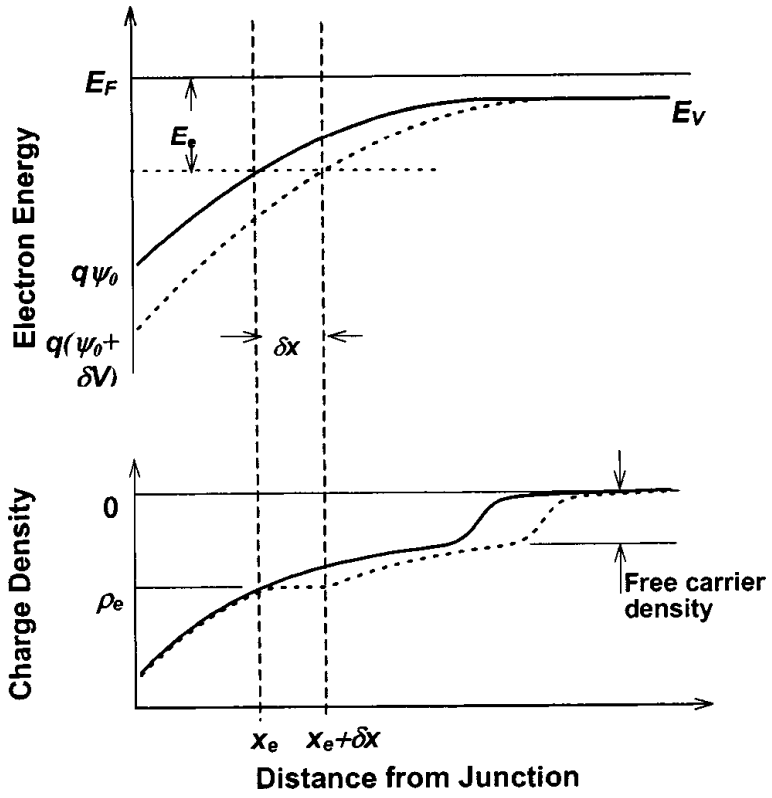

Figure 3.9: Upper curve shows the change in band bending due to a small bias applied to the sample. Solid line before and dashed lines after application of δV. Lower curves shows the corresponding charge densities. E_e is determined by measurement conditions.

At a given ω_{ac}, T and DC bias, position x_e is defined as the location at which $E_F - E_v = E_e$. Between the junction and the point x_e we have $E_F - E_v > E_e$ and in this condition the occupation of any gap states usually do not have time to follow the small signal ac. At larger distances from the junction, gap states can dynamically respond to our ac signal.

Considering the dc potential at the interface without applied bias, $\psi_0(x = 0)$ is calculated as follow:

$$\psi_0(0) = \int_0^\infty x\frac{\rho_0(x)}{\epsilon}\,dx = \int_0^{x_e} x\frac{\rho_0(x)}{\epsilon}\,dx + \int_{x_e}^\infty x\frac{\rho_0(x)}{\epsilon}\,dx \tag{3.22}$$

[1]We refer to the valence band because CdTe is a p-type material.

In presence of an applied δV, the point x_e moves away from junction and the new cross point is defined as $x_e + \delta x$ (see figure 3.9). Considering a δV applied for a time of order of $\frac{1}{\omega_{ac}}$, the charge density between the interface and x_e remains unchanged. Between x_e and $x_e + \delta x$ occupation of states is emission limited so the charge density is roughly the same of the charge at x_e before applying δV and remains constant in this part of the device. We can assume negligible any variation of semiconductor properties on a length scale of δx, hence beyond x_e we can consider $\rho(x) = \rho_0(x - \delta x)$. We can calculate $\psi(0)$ as:

$$\psi(0) = \int_0^{x_e} x\frac{\rho_0(x)}{\epsilon}\,dx + \int_{x_e}^{x_e+\delta x} x\frac{\rho_e}{\epsilon}\,dx + \int_{x_e+\delta x}^{\infty} x\frac{\rho_0(x-\delta x)}{\epsilon}\,dx \tag{3.23}$$

The total change of the charge δQ caused by the applied δV is:

$$\delta Q = A\rho_e\delta x \tag{3.24}$$

Combining 3.22 and 3.23 we obtain

$$\begin{aligned}\delta V &= \psi(0) - \psi_0(0)\\ &= \frac{\rho_e}{2\epsilon}[(x_e+\delta x)^2 - x_e^2] + \int_{x_e}^{\infty}\delta x\frac{d^2\psi}{dx^2}\,dx\\ &= \frac{\rho_e}{2\epsilon}(2x_e\delta x + \delta x^2) - \delta x F_e\end{aligned} \tag{3.25}$$

where

$$F_e = -\left.\frac{d\psi}{dx}\right|_e \tag{3.26}$$

is the definition of the electric field at the point x_e.
Solving equation 3.25 by δx we have:

$$\begin{aligned}\delta x &= \left(\frac{\epsilon}{\rho_e}F_e - x_e\right)\left(1 - \sqrt{1 + \frac{2\rho_e\epsilon\delta V}{(\epsilon F_e - \rho_e x_e)^2}}\right)\\ &\approx \frac{\epsilon}{\epsilon F_e - \rho_e x_e}\delta V - \frac{\rho_e\epsilon^2}{2(\epsilon F_e - \rho_e x_e)^3}\delta V^2 + \dots\end{aligned} \tag{3.27}$$

Substituting equation 3.24 in 3.27 we can finally point out the taylor series expansion form:

$$\begin{aligned}\frac{\delta Q}{\delta V} &= \frac{A\rho_e\epsilon}{\epsilon F_e - \rho_e x_e} - \frac{A\rho_e^2\epsilon^2}{2(\epsilon F_e - \rho_e x_e)^3}\delta V + \dots\\ &= C_0 + C_1 dV + C_2(dV)^2\dots\end{aligned} \tag{3.28}$$

Hence putting equation 3.28 in terms of a positive quantity $|\rho_e|$ so we can apply this results for both p-type and n-type semiconductors we obtain:

$$\begin{aligned}C_0 &= \frac{A|\rho_e|\epsilon}{\epsilon F_e + |\rho_e|x_e}\\ C_1 &= -\frac{A\rho_e^2\epsilon^2}{2(\epsilon F_e + |\rho_e|x_e)^3}\end{aligned} \tag{3.29}$$

The term C_0 is the same value obtained by capacitance voltage technique. Shallow defects combining C_0 and C_1 can be calculated as:

$$N_{DL} \triangleq \frac{|\rho_e|}{q} = -\frac{C_0^3}{2q\epsilon A^2 C_1} \tag{3.30}$$

In practice for each V_{DC} bias and fixed T, f_{ac}, we apply a superposition of different amplitudes of V_{ac}, typically from 50mV to 350mV with a step of 50mV; these 7 values are interpolated with n-polynomial curve fitting in order to obtain the Taylor series expansion described in equation 3.28. With coefficient C_0 and C_1 extracted from fitting we can calculate N_{DL} at the distance x_e from the junction. It is worth to underline that theorical derivation of C_0 and C_1 assumes that applied δV is asimmetric respect V_{DC} because the point x_e is moved only between x_e and $x_e + \delta x$. However applied V_{ac} is a sinusoidal signal over the DC bias and would move x_e in a range between $x_e - \delta x$ and $x_e + \delta x$. So each time ac amplitude is increased, dc value must be decreased by the same value because it is required a constant maximum applied voltage $dc + ac$:

$$\begin{cases} V_{max_1} = \hat{V}_{ac_1} + V_{DC_1} \\ V_{max_2} = \hat{V}_{ac_2} + V_{DC_2} \\ \quad \vdots \\ V_{max_7} = \hat{V}_{ac_7} + V_{DC_7} \end{cases} \quad \Rightarrow \quad V_{max_1} = V_{max_2} = \ldots = V_{max_7} \tag{3.31}$$

Equation 3.31 ensure that all measure of capacitance used for n-polynomial curve fitting are referred to the same point x_e, see figure 3.10 for a graphical representation of the applied bias.

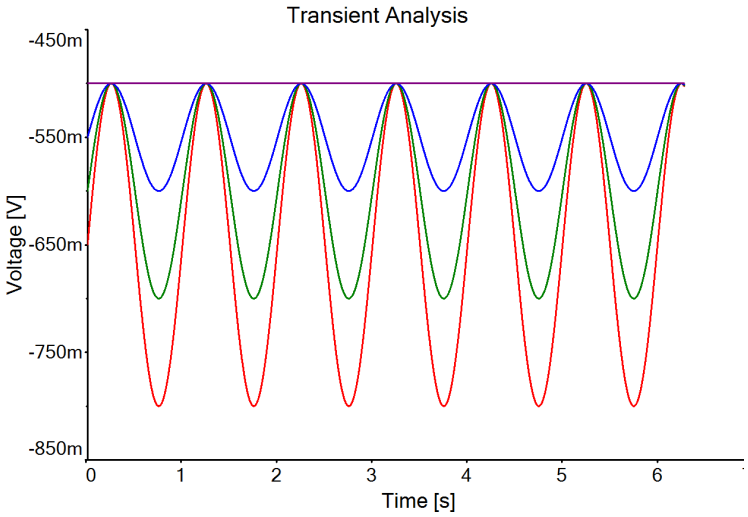

Figure 3.10: Both dc and ac applied signal must be changed in tandem so that the position x_e remains fixed while sweeping amplitude of V_{ac}.

3.5 External and Internal Quantum Efficency

The External Quantum Efficiency (EQE) is defined as:

$$EQE(\lambda) = \frac{J_{sc}(\lambda)}{q\phi_{in}(\lambda)} \tag{3.32}$$

EQE represent the fraction of charge carriers collected per incident photon and it is determined by measuring the short circuit current response to illumination using different monochromatic lights.

EQE of our samples are performed with LOANA system (figure 3.11) of Padua University at Department of Information Engineering laboratories. EQE data are kindly provided by PhD student Marco Barbato and Professor Matteo Meneghini. The measurement system consists of three units.

On the left are located the supply unit with monochromatic light source (xenon arc light source, tungsten halogen light source, bias light source, monochromator...), vacuum pump, thermostat and power supplies.

Compartment in the center contains xyz measurement table, cameras, optics and motor stop.

On the right we have the control rack with measurement and control electronics, PC operation panel and emergency stop.

Figure 3.11: Instrumentation used to perform QE measurement.

EQE set up uses a reference cell with a known EQE_{cal} to determine the sample EQE_{sample}. Moreover a correction of the fluctuation in the light intensity between calibration and measurement is performed dividing the signals $S_{Jsc,sample}$ and $S_{Jsc,cal}$ by the signal from the monitor diode S_{mon}. Monitor diode is located inside the flash channel. Hence EQE is calculated as follow:

$$EQE_{sample}(\lambda) = EQE_{cal}(\lambda) \cdot \frac{S_{Jsc,sample}(\lambda)}{S_{Jsc,cal}(\lambda)} \cdot \frac{S_{mon,cal}(\lambda)}{S_{mon,sample}(\lambda)} \tag{3.33}$$

where

- EQE_{sample} = desired EQE of the sample
- EQE_{cal} = given EQE of the internal reference cell
- $S_{Jsc,sample}$ = measured signal of the sample
- $S_{Jsc,cal}$ = measured signal of the internal reference cell
- $S_{mon,cal}$ = measured monitor signal of the internal reference cell
- $S_{mon,sample}$ = measured monitor signal of the sample

In order to obtain the Internal Quantum Efficiency (IQE) we used an indirect calculation combining EQE information with the integral reflectance of the sample (REFL). This measurement is performed with monochromatic illumination and an integrating sphere (figure 3.12). It is defined as the fraction of light reflected per incident photon. Reflectance calculation algorithm is the following:

$$R = (R_{99} - R_0) \cdot \frac{S - S_0}{(S_{99} - S_0)} \cdot \frac{1}{M_R} \tag{3.34}$$

where parameters are defined as:

- R = measured reflectance for the sample
- R_0 = given reflectance for the dark reference
- R_{99} = given reflectance for the calibrated 99% reflectance standard
- S = signal measured for the sample
- S_0 = signal measured for the dark reference
- S_{99} = signal measured for the 99% reflectance standard
- M_R = Correction factor for the average sphere reflectance (which depends on the reflectance of the port)

IQE is defined as:

$$IQE = \frac{electrons/sec}{absorbedphotons/sec} = \frac{EQE}{1 - Reflection - Transmission} \tag{3.35}$$

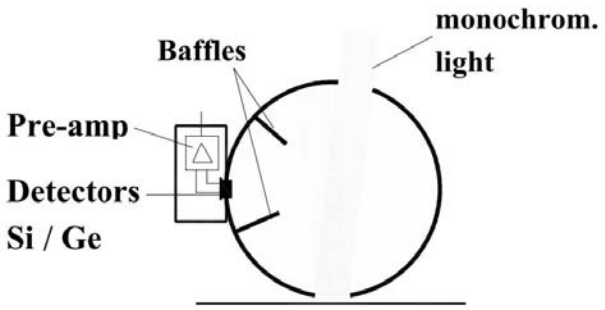

Figure 3.12: Integrating sphere used to calculate the sample reflectance. Monochromatic light illuminates the sample through the sphere input port. The reflected light is collected by the sphere and reflected until measured by detectors. Incidence angle is tilted by 8° to detect both specular and diffuse components preventing the specular component from leaving the sphere through the input port.

Chapter 4

Effects Of The Treatment Temperature

All the measurements explained in chapter 3 are used to study samples made at different treatment temperature: specifically 310°C, 330°C, 360°C, 380°C, 395°C, 410°C. This chapter reports results and information about the effects of temperature on the reaction between $CdCl_2$ and the CdS/CdTe stack.

4.1 Sample preparation

Deposition of $CdCl_2$ follows the procedure explained in paragraphs 2.6 and 2.7. We deposit 40 drops and dry the surface heating the sample at 55°C, then we choose one of the temperature mentioned to perform the activation treatment. Sample is etched and put in a vacuum chamber for copper and gold deposition. Finally back contact is annealed at 190°C. Many samples per temperature are made in order to obtain a good statistical representation of device performance.

It is worth to note that temperature ranging from 310°C to 410°C are nominal values set in oven parameters as the internal thermocouple measures the temperature in the oven. However the sample is closed in a glass petri so we checked the real temperature putting a second thermocouple inside the petri. Figures 4.1-4.6 reports the ramp temperature of the treatments. Real overshoot measurements are roughly 40°C−50°C higher than the set point, while in steady-state thermocouple inside the petri measures 20°C−30°C more than the set point. Table 4.1 reports more precisely a comparison between nominal value and real value.

In this chapter we will always refer to the nominal value of temperature when comparing different treatments.

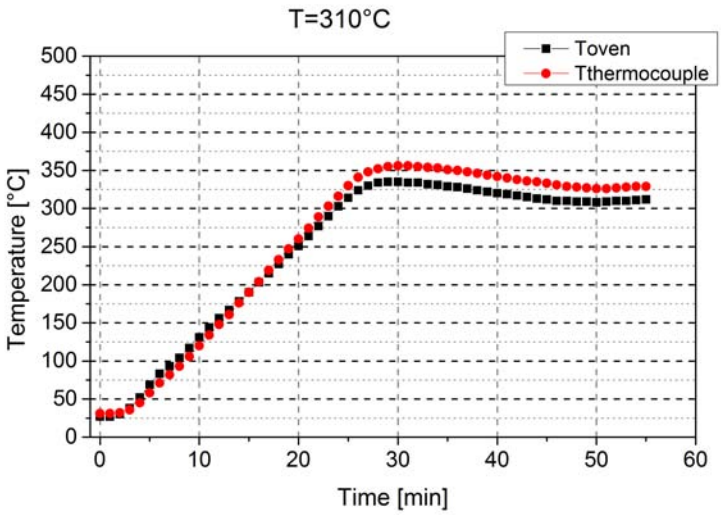

Figure 4.1: Ramp at 310°C.

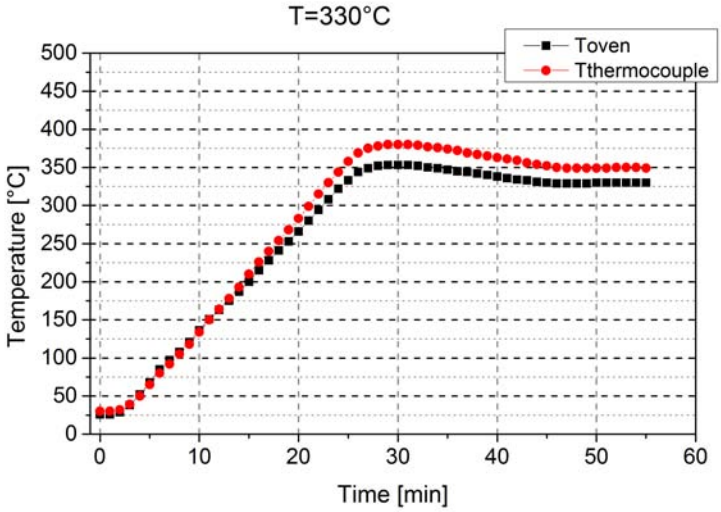

Figure 4.2: Ramp at 330°C.

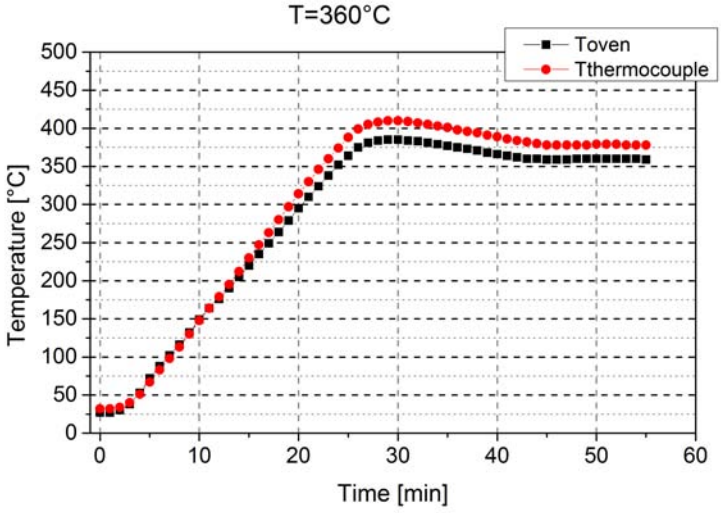

Figure 4.3: Ramp at 360°C.

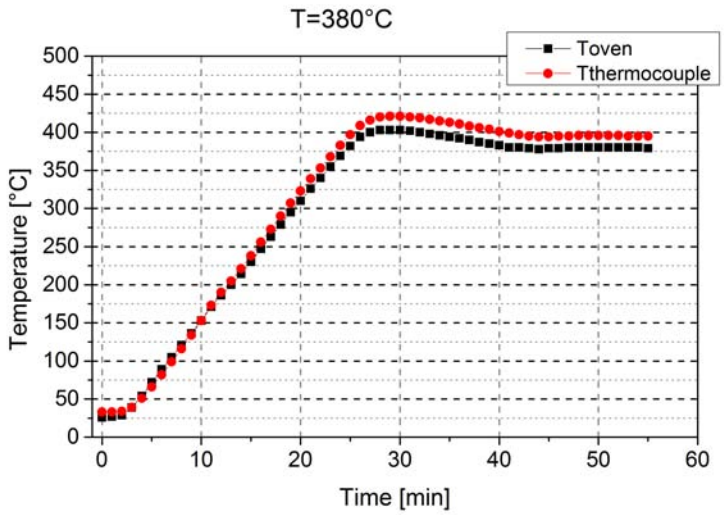

Figure 4.4: Ramp at 380°C.

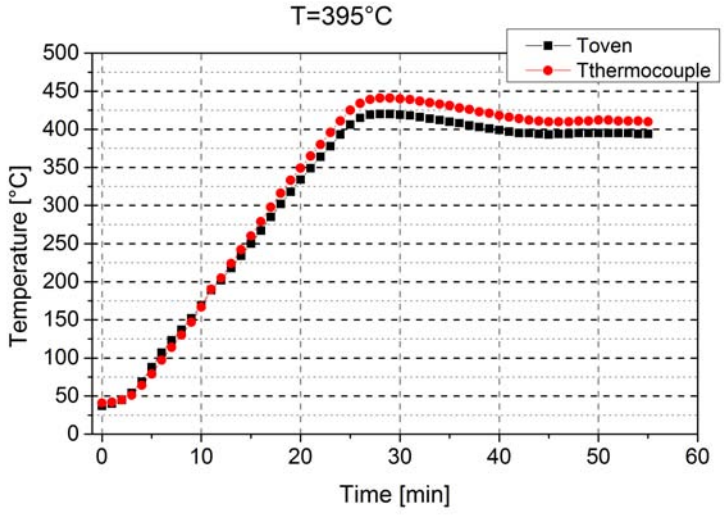

Figure 4.5: Ramp at 395°C.

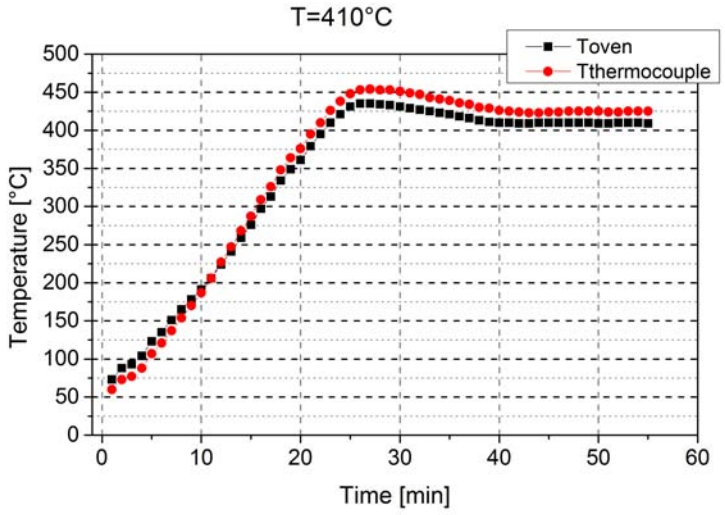

Figure 4.6: Ramp at 410°C.

Nominal temperature	Overshoot		Steady-state	
	T	Δ T	T	Δ T
310°C	356 °C	+46°C	329°C	+19°C
330°C	380 °C	+50°C	350°C	+20°C
360°C	410 °C	+50°C	378°C	+28°C
380°C	421 °C	+41°C	395°C	+15°C
395°C	441 °C	+46°C	410°C	+15°C
410°C	454 °C	+44°C	425°C	+15°C

Table 4.1: Summary of activation treatment temperatures measured by a thermocouple located inside the petri where reaction between CdTe and $CdCl_2$ occurs.

4.2 J-V

To underline the importance of the activation treatment step process, we made two samples without treating CdTe film. In the first case we deposited copper and gold directly on the as deposited CdTe surface. In the second we etched CdTe film before back contact deposition. Both samples show an IV characteristic typical of a resistance as the current signal is not rectified (figure 4.7). Hence a deposition of CdTe on a CdS film is not sufficient to form a solar cell. Even if at low temperature, activation treatment is fundamental to start the reaction that creates the intermixing layer between CdS and CdTe, otherwise devices act as a resistance instead of a diode.

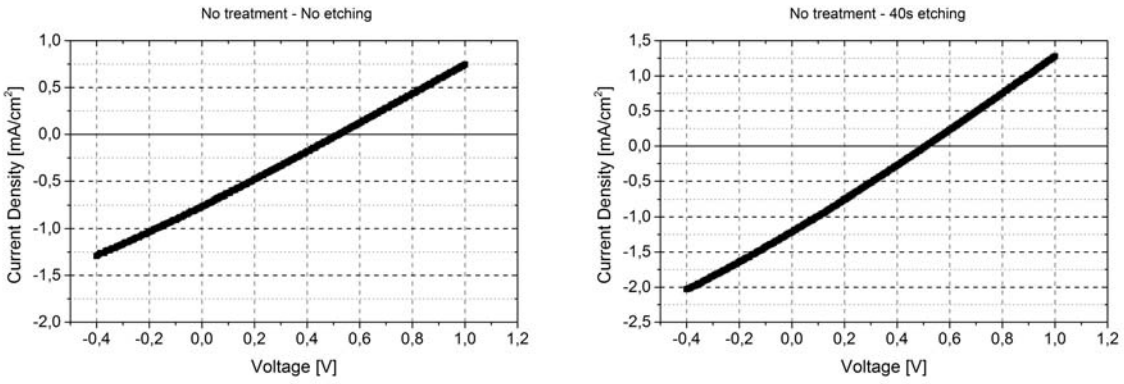

Not treated, not etched

Not treated, 40s etching

Figure 4.7: These samples are made without $CdCl_2$ activation treatment. Sample on the left is made by depositing back contact directly on the as-deposited CdTe surface, while sample on the right is etched before back contact deposition.

Statistical results of I-V curves are shown in figures 4.8, 4.9, 4.10 and 4.11. Efficiency sensibly increases changing the treatment temperature from 310°C to 360°C and slightly increase up to 395°C which represents the best case. The standard deviation also increases with temperature indicating a reduced uniformity

of the samples. At 410°C efficiency is lower due to a strong treatment that spoils the CdS surface, all samples show white spots on the frontside, fill factor is the worst of all temperature suggesting low shunting resistance. We also have higher standard deviation of fill factor and V_{oc} hence we can say that process becomes unstable at this temperature.

V_{oc} is highly reproducible and is affected by a low standard deviation. Mean value shows a tendency to increase with temperature. We notice an exception at 380°C: V_{oc} is slightly lower than a treatment made at 360°C but fill factor increases and overcome the loss of V_{oc} at this treatment temperature. Comparing V_{oc} and efficiency graphs we can observe very similar curves, this fact suggests that treatment temperature mainly affect this parameter. Referring to best cases we can see a monotonic growth of V_{oc} with temperature.

J_{sc} grows from 310°C to 360°C and then stays almost constant. This could be related to grains size (see paragraph 4.3) that also follow this trend. As grains boundaries work like electron-hole recombination center, J_{sc} increases because of grains growth. Moreover we can observe that standard deviation stays almost constant, this parameter is the less affected by the treatment temperature[1].

Fill factor parameter is more difficult to reproduce, probably it is more sensible than other parameters to any variations in the whole step process, hence is more unpredictable and it is the main cause of the efficiency standard deviation increment with higher treatment temperature. At 395°C mean value of fill factor is lower than 380°C but as a consequence of an improved V_{oc} we get the best efficiencies at this temperature.

Referring to best cases we can achieve high fill factors with both 380°C and 395°C, see table 4.2, however samples treated at 395°C have higher performance due to higher V_{oc}. Figures 4.12-4.17 show efficiency best case for each temperature. We can observe that 310°C and 330°C have the same current of $22.5\frac{mA}{cm^2}$ while other treatment temperature have higher values. As said before there are small differences between sample made at 360°C, 380°C, 395°C see figure 4.18. All curves are affected by roll over. Causes of different quality contact at 1V have not been analyzed, this problem goes beyond the scope of this work.

Sample V4701 T=380°C		V4702 T=395°C	
V_{oc}	824mV	V_{oc}	859mV
J_{sc}	$22.3\frac{mA}{cm^2}$	J_{sc}	$23.4\frac{mA}{cm^2}$
FF	73.7%	FF	73.7%
η	13.6%	η	14.8

Table 4.2: These two samples show the highest FF achieved in this work. As they are treated at different temperatures, we can say that previous step process affect this parameter more than others, while temperature affects mainly the V_{oc}.

[1]See also paragraph 4.6 to compare J_{sc} measurements performed with LOANA system.

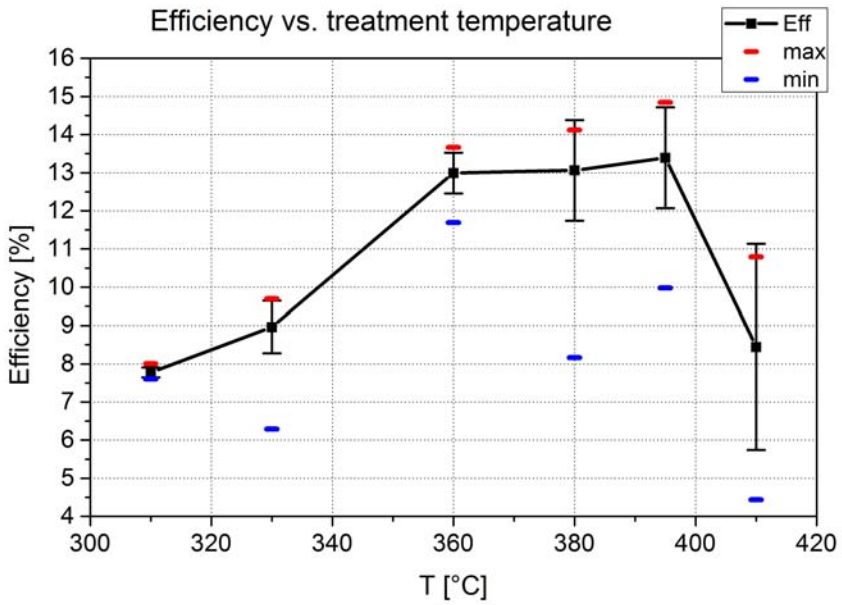

Figure 4.8: Statistic of η. Efficiency sensibly increases with temperature up to 360°C, then slightly increase up to 395°C and then fall down at 410°C because of a spoiled frontside.

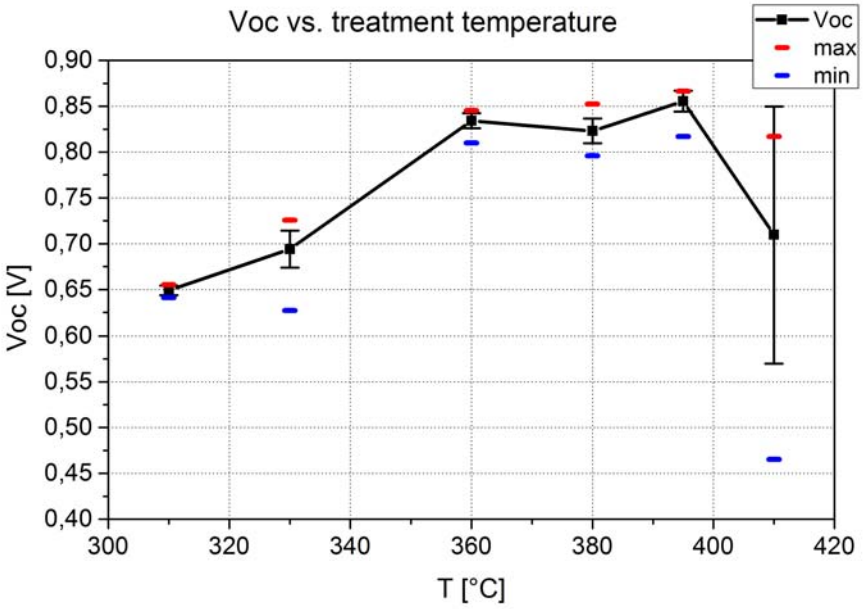

Figure 4.9: Statistic of V_{oc}. This parameter is strongly connected with efficiency curve. Activation treatment mainly affect this parameter.

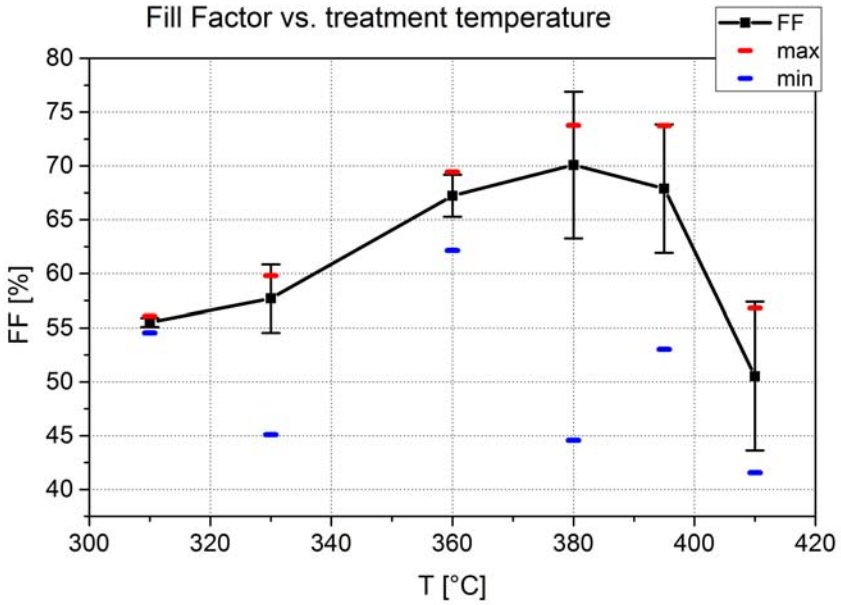

Figure 4.10: Statistic of Fill Factor. This parameter is the main responsible of efficiency standard deviation increment with treatment temperature.

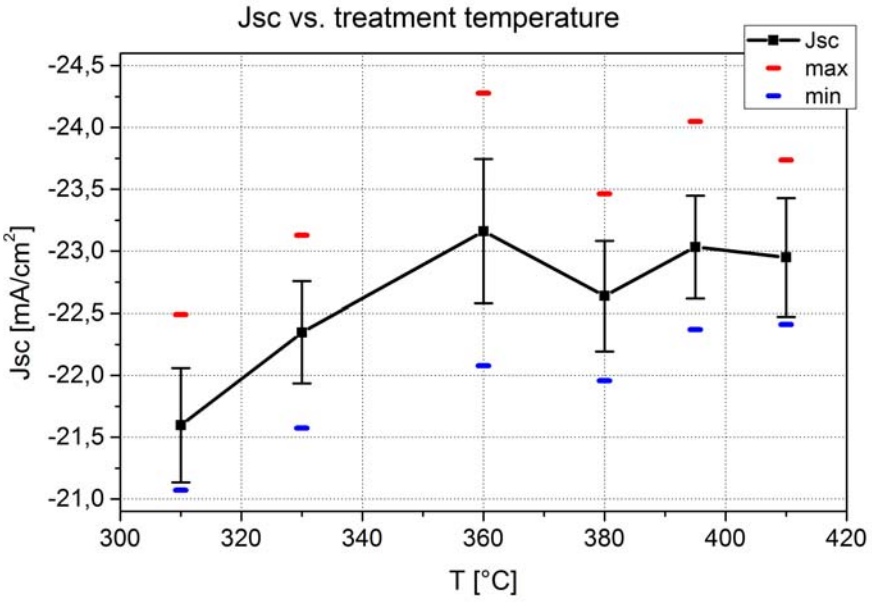

Figure 4.11: Statistic of J_{sc}. Current density increases up to 360°C and then stays almost constant. It is connected with grains size growth due to activation treatment.

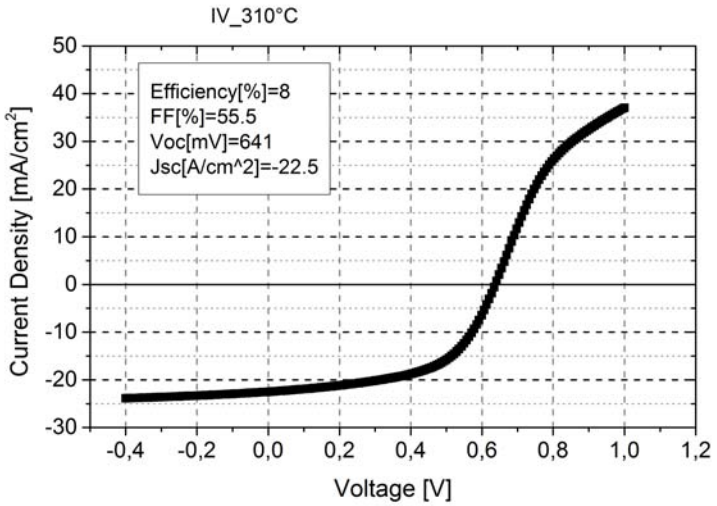

Figure 4.12: IV at 310°C

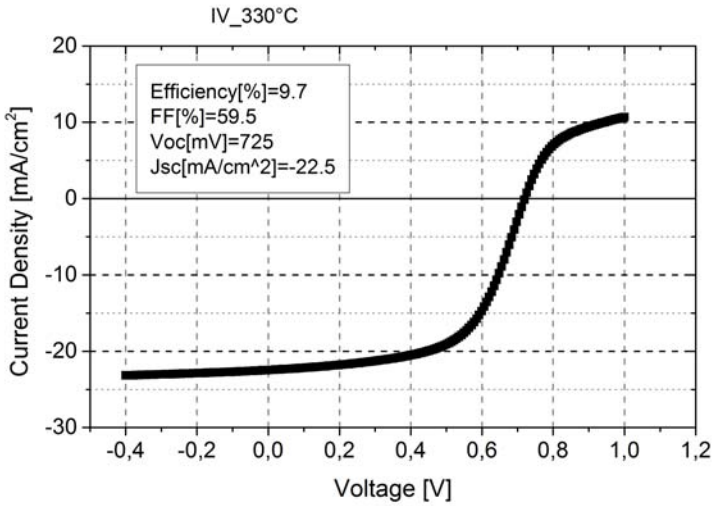

Figure 4.13: IV at 330°C

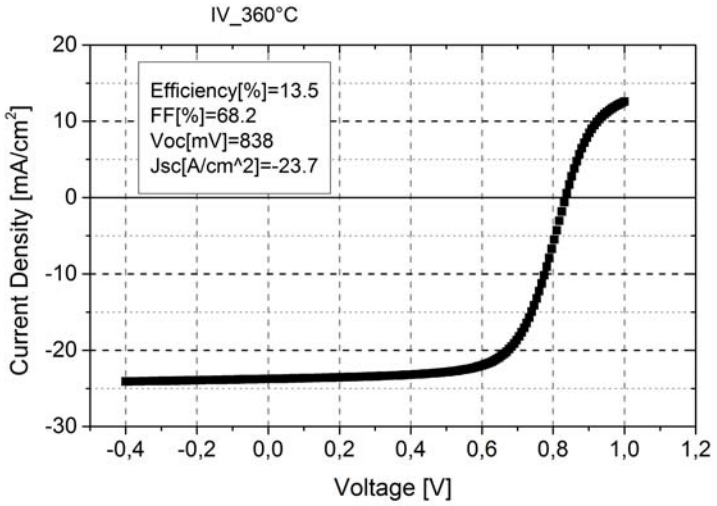

Figure 4.14: IV at 360°C

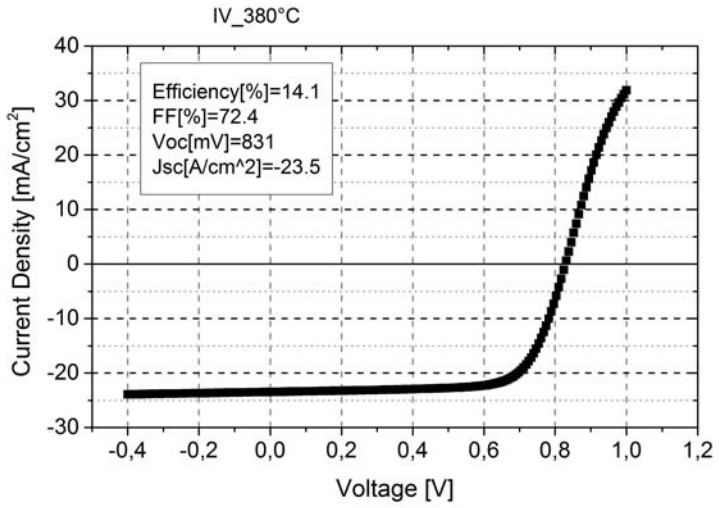

Figure 4.15: IV at 380°C

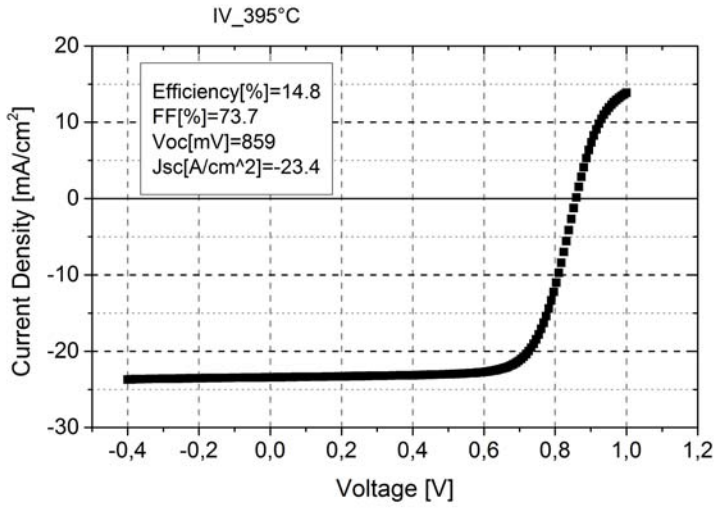

Figure 4.16: IV at 395°C

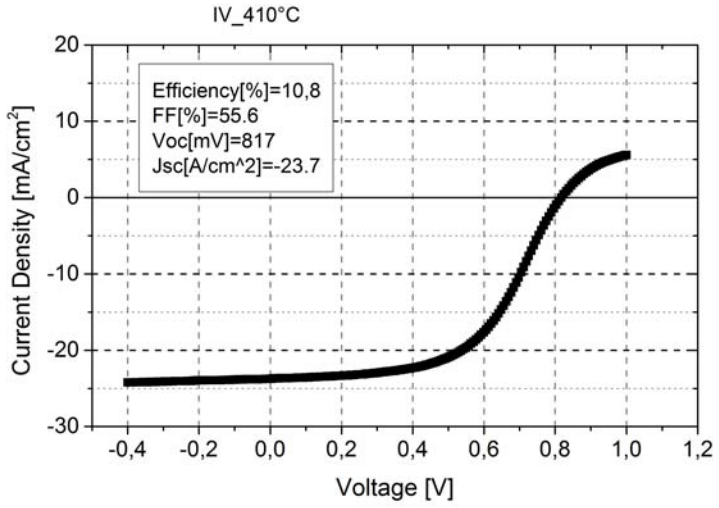

Figure 4.17: IV at 410°C

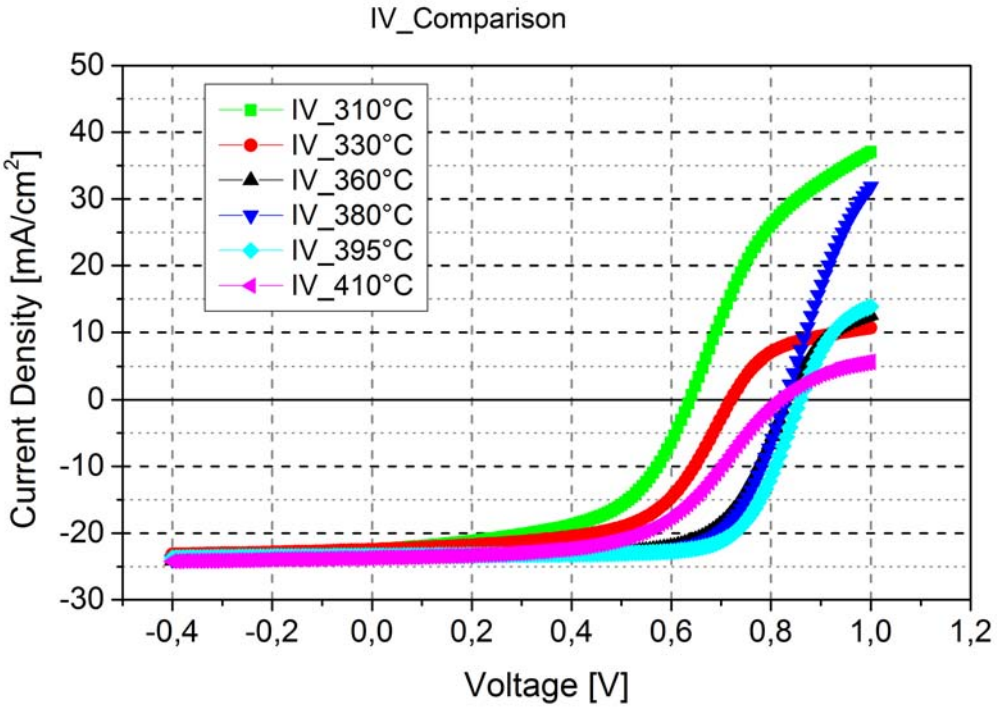

Figure 4.18: This figure shows previous J-V together. We can observe that curves shift to the right increasing treatment temperature. Samples made at 360°C, 380°C, 395°C are very similar and have high efficiencies.

4.3 AFM images

Morphology of samples treated at 310°C (figure 4.19) is not that different from as deposited samples. Grains size is $\leq 1\mu m$. Increasing temperature up to 330°C (figure 4.20) can improve grains size up to $3\mu m$, however a lot of grains with $1\mu m$ of diameter are still present. At 360°C (figure 4.21) recrystallization of CdTe becomes more noticeable, grains range from $1\mu m$ to $5\mu m$.

As said in the previous paragraph a consequence of CdTe growth is an increment of J_{sc}. Sample treated at 380°C (figure 4.22) shows $1\mu m$-$7\mu m$ grains size and at higher temperatures 395°C-410°C (figure 4.23-4.24) both shows $1\mu m$ to $10\mu m$ grains diameter. Moreover, increasing temperature, smaller grains tend to decrement in concentration as recrystallization becomes more effective.

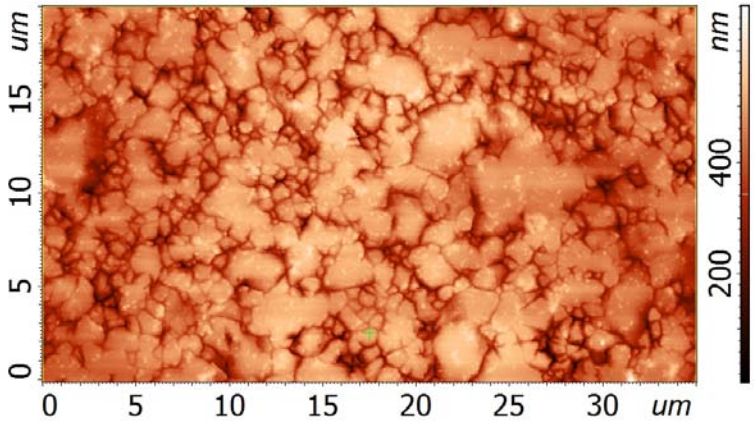

Figure 4.19: AFM image of sample treated at 310°C. Grains size is less than 1μ.

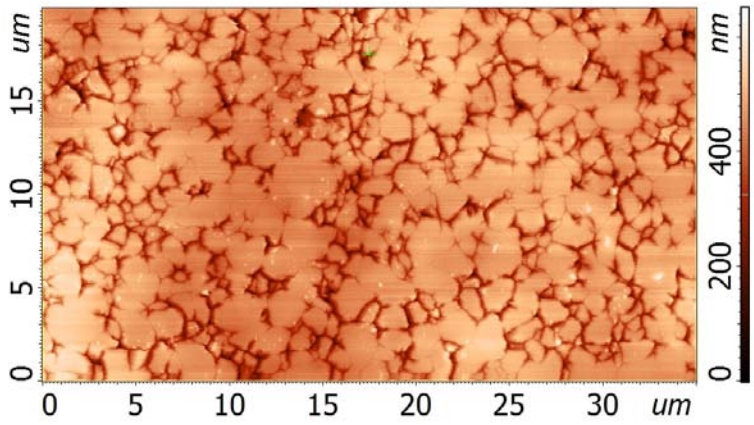

Figure 4.20: AFM image of sample treated at 330°C. Grains size is less than 3μ.

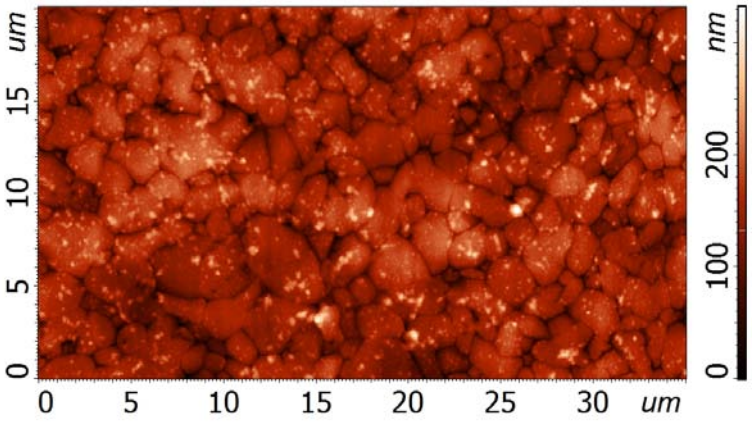

Figure 4.21: AFM image of sample treated at 360°C. Grains size ranges from 1μ to 5μ.

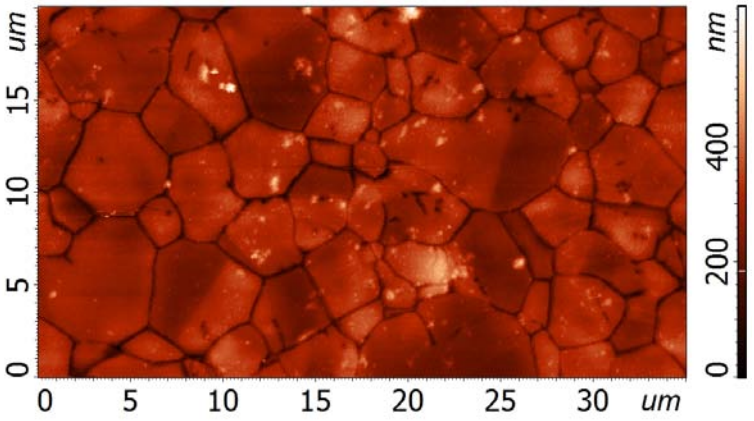

Figure 4.22: AFM image of sample treated at 380°C. Grains size ranges from 1μ to 7μ.

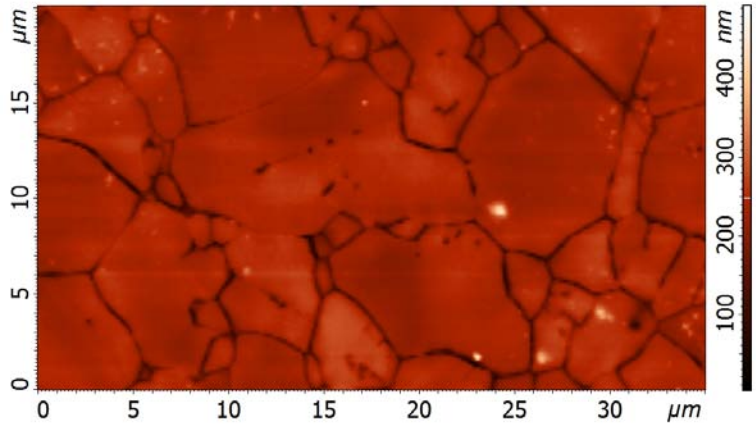

Figure 4.23: AFM image of sample treated at 395°C. Grains size ranges from 1μ to 10μ.

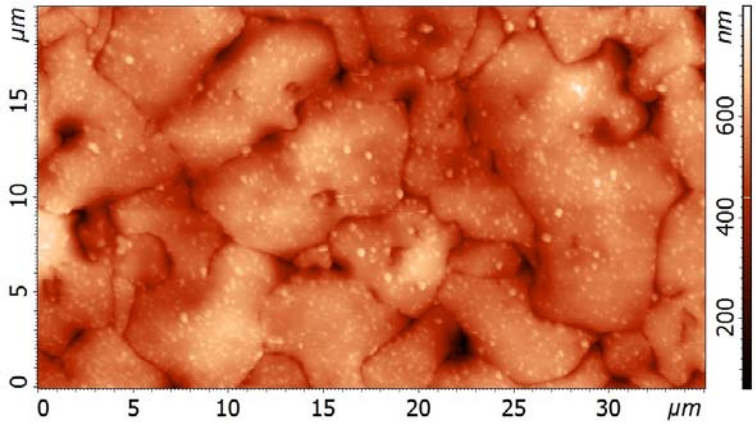

Figure 4.24: AFM image of sample treated at 410°C. Grains size ranges from 1μ to 10μ.

4.4 XRD and Nelson Taylor plot

X-Ray diffraction spectroscopy is used to detect orientation of crystal planes, analyzing spectra of our samples we can collect information about physical transformation. At 310°C and 330°C XRD show a high (111) preferred orientation similar to as-deposited samples, this highlight a low effect of $CdCl_2$ that doesn't change the preferred orientation. At 360°C other peaks become more intense, especially (311) and (422), but still smaller than (111) orientation. Also (531) peak appears at this temperature. From 380°C to 410°C we have high reorientation that suggests a higher treatment effect, (111) peak is more or less the same as (311) and (422). At 410°C we notice (440) peak that was not detectable at lower temperatures.

From XRD data we can also calculate the lattice parameter with Nelson-Taylor plot (table 4.3). Extracted data show an increasing value from 310°C to 360°C that measure respectively 6.484Å, 6.485Åand 6.488Å. Then stays constant and samples treated at 380°C and 395°C have the same lattice parameter (6.488Å), at 410°C instead the value drops at 6.478Å. This suggest that 6.488Åis the best value of lattice parameter that minimize the strains due to CdS/CdTe lattice mismatch as typical efficiencies at these three temperatures exceed 13%, however if temperature is too high, lattice parameter decrease because of a strong intermixing between CdS and CdTe spoiling the junction.

Temperature	a (Å)	std
310°C	6.484	$2{\cdot}10^{-3}$
330°C	6.485	$1.1{\cdot}10^{-3}$
360°C	6.488	$1.3{\cdot}10^{-3}$
380°C	6.488	$1.3{\cdot}10^{-3}$
395°C	6.488	$1.4\ {\cdot}10^{-3}$
410°C	6.478	$4.7{\cdot}10^{-3}$

Table 4.3: Lattice parameter at different treatment temperature

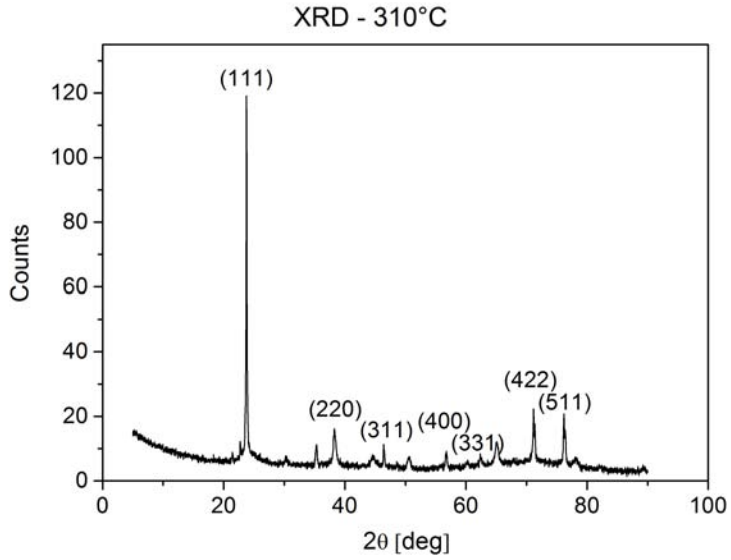

Figure 4.25: XRD of samples treated at 310°C. Sample shows a (111) preferred orientation. Activation treatment is too weak to perform a significant transformation of CdTe layer.

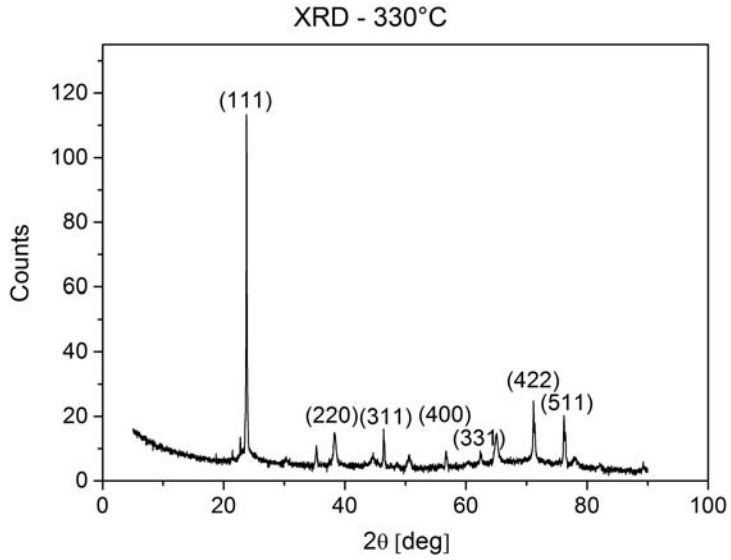

Figure 4.26: XRD of samples treated at 330°C. Small peaks slightly increase.

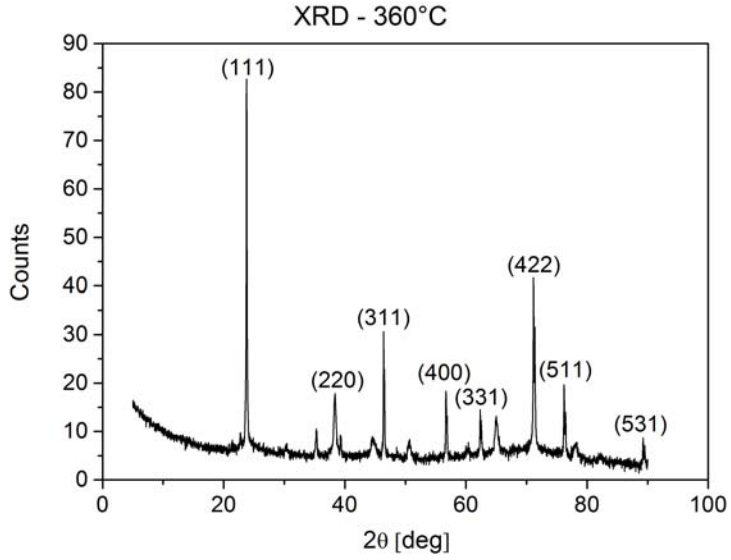

Figure 4.27: XRD of samples treated at 360°C. All peaks are clearly visible, peak (531) appears at this treatment temperature.

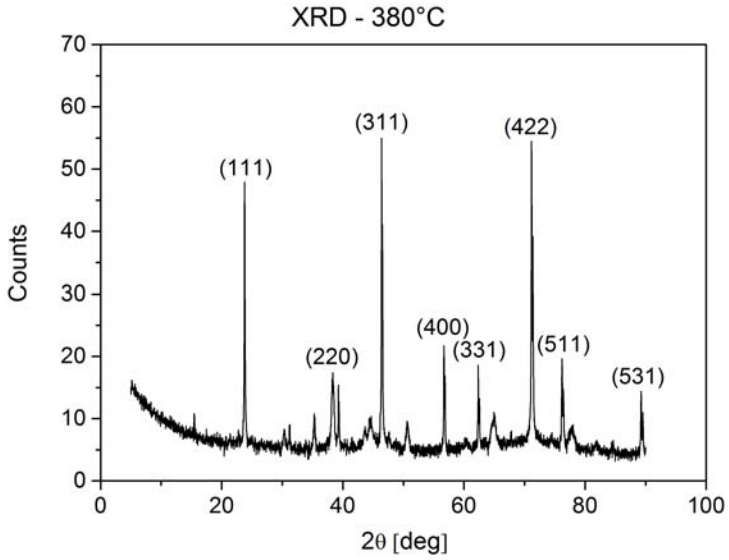

Figure 4.28: XRD of samples treated at 380°C. (111) preferred orientation is lost.

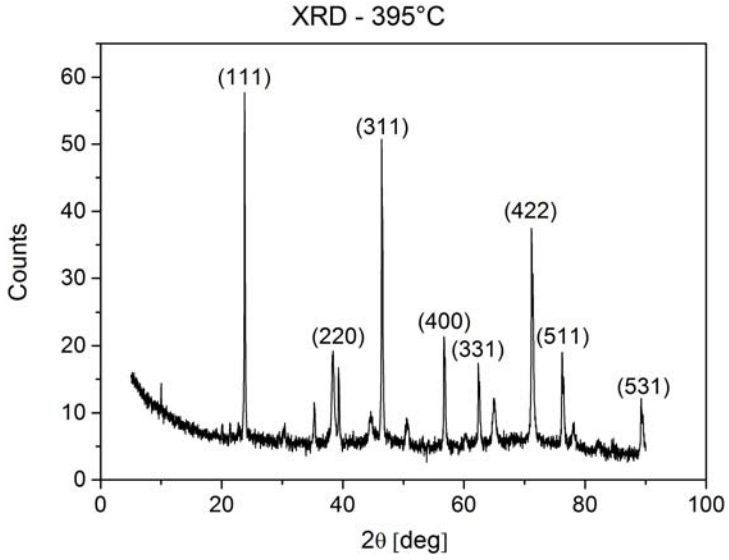

Figure 4.29: XRD of samples treated at 395°C. All peaks randomly increase.

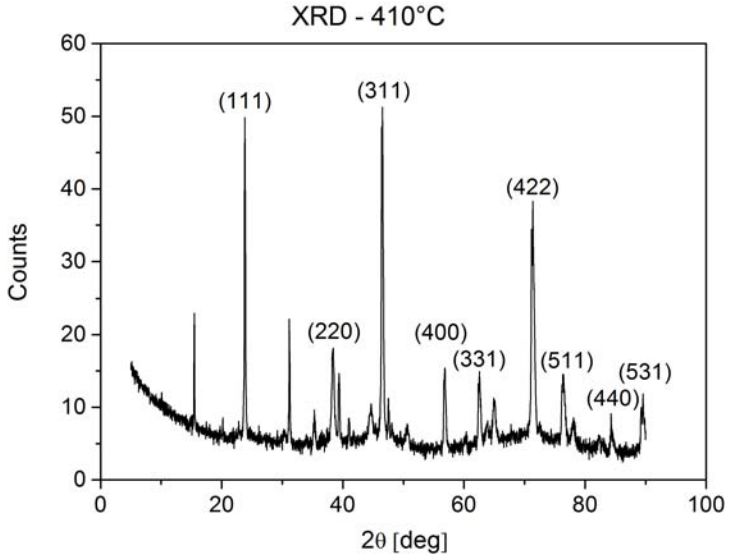

Figure 4.30: XRD of samples treated at 410°C. New peak (440) appears at this temperature.

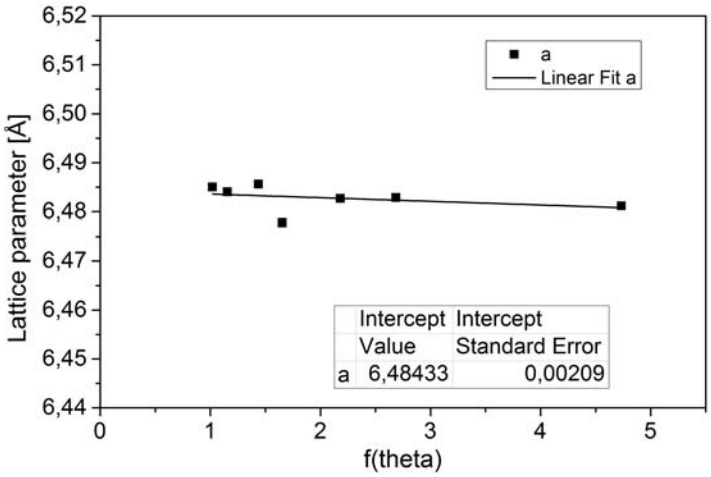

Figure 4.31: NTP of samples treated at 310°C.

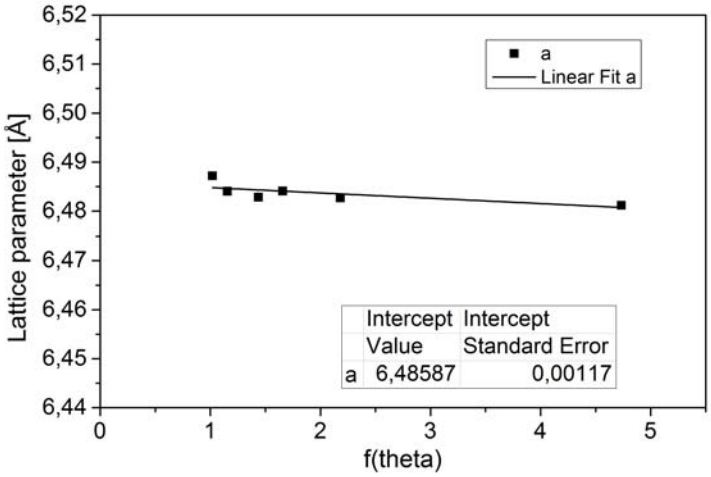

Figure 4.32: NTP of samples treated at 330°C.

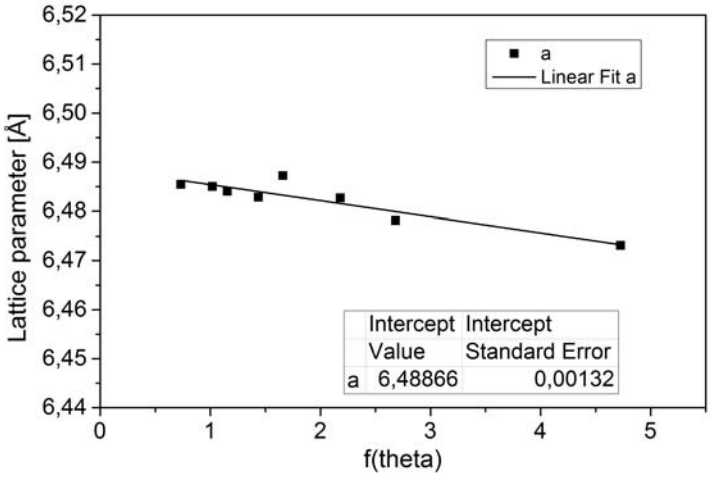

Figure 4.33: NTP of samples treated at 360°C.

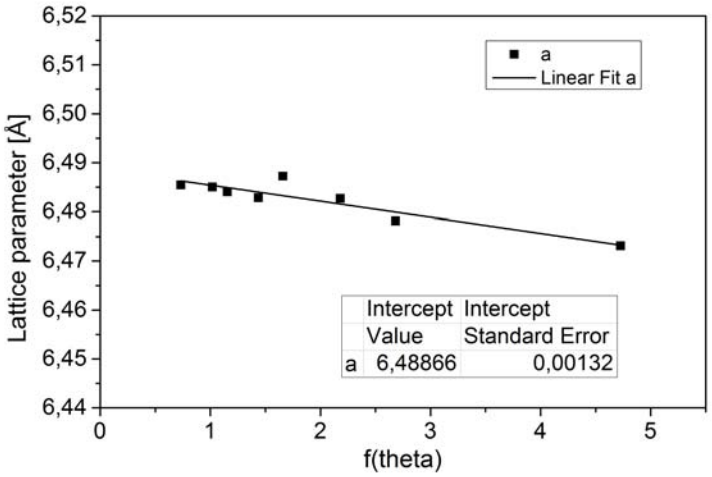

Figure 4.34: NTP of samples treated at 380°C.

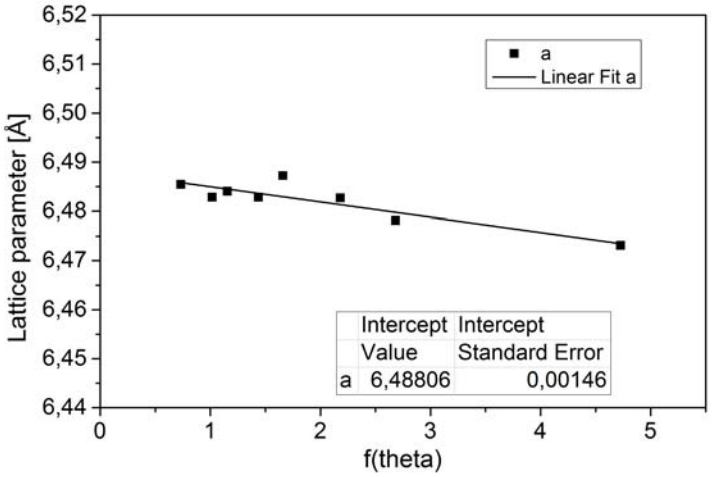

Figure 4.35: NTP of samples treated at 395°C.

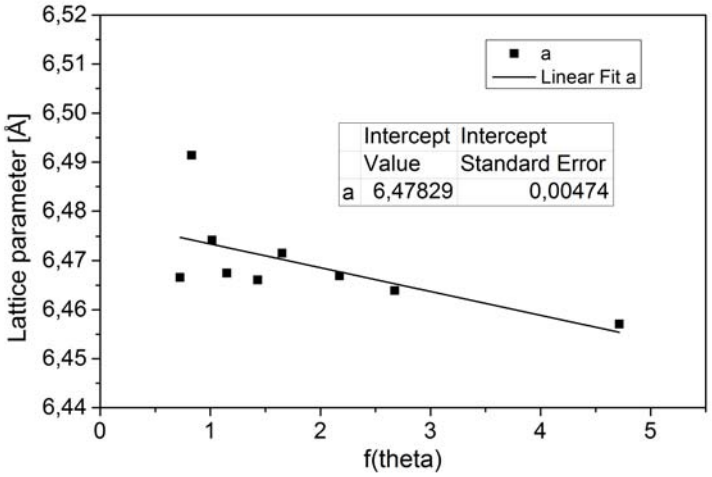

Figure 4.36: NTP of samples treated at 410°C.

4.5 CV-DLCP

As described in paragraph 3.4 we can investigate profile of dominant defects with this technique. All these measures are performed at room temperature in dark conditions. For each sample, measurement of CV and DLCP are made at 10kHz, 50kHz, 100kHz, 1MHz. By changing V_{ac} signal frequency we can change the limiting energy and reduce or freeze out the effect of the dominant defect at room temperature. CV profile is plotted with empty dots, while N_{DL} is plotted with full square.

4.5.1 Treatment temperature: 395°C

This is the best treatment temperature, measured profile are showed in figure 4.41. The DLCPs value at all the frequencies ranges between $10^{14}cm^{-3}$ in the bulk CdTe and $10^{15}cm^{-3}$ approcaching the junction. Shallow defects profile at 10kHz, 50 kHz, 100 kHz are roughly the same suggesting that the dominant defect is fast enough to follow the applied ac signal. Increasing the frequency at 1MHz we have a small reduction of N_{DL} because less shallow acceptor defects are able to follow the applied signal. Also CV profile almost follows this trend, deep defects, calculated as the difference between CV profile and DLCP profile, (figure 4.47) shows roughly the same positioning of the peak of deep defects and the same peak value, roughly $4 \cdot 10^{14}cm^{-3}$. As described in paragraph 3.4 DLCP measures the concentration of shallow defects at the point x_e, hence we can localize defects at that distance from the junction; in CV profile deep defects affect the measurement farther than their real localization in the device. Moreover as the contribution of deep defects has a maximum, we can say that deep defects are spatially distributed near the junction.

4.5.2 Treatment temperature: 410°C

This sample shows a higher density of shallow defects that follows a trend with frequency. As net acceptor concentration increases with frequency, we can conclude that dominant defects are donor type. Equation 3.18 in paragraph 3.4 neglects contribution of donor defect: more precisely we measure $N_A - N_D$, CdTe is a p-type semiconductor so $N_A > N_D$, hence for compensation we obtain a concentration of acceptor defects. In this case we point out the presence of donor defects as we measure an increment of the net acceptor density increasing the frequency, hence we are limiting the response of donor defects and decreasing N_D. Deep defects contribution is higher than the sample treated at 395°C. Deep defect peak is localized at $1.1\mu m$ from the junction at lower frequencies while at 1MHz measured concentration slightly decreases and shifts the maximum at $1.5\mu m$, so they have a different behavior from shallow defects. At 410°C treatment increase shallow defects, at $1\mu m$ of distance considering the 100kHz curve $N_{DL,395°C} \approx 5 \cdot 10^{14}cm^{-3}$ while $N_{DL,410°C} \approx 1 \cdot 10^{15}cm^{-3}$; on the other hand also deep defects increases, comparing peaks magnitude obtained by the measurement $N_{deep,395°C} \approx 2 \cdot 10^{14}cm^{-3}$ and $N_{deep,410°C} \approx 1 \cdot 10^{15}cm^{-3}$. Hence increment of deep defects vanishes the increment of shallow defects, so device performance is worse at this treatment temperature.

4.5.3 Treatment temperature: 380°C

Near the interface shallow defects are the same of the sample made at 395°C: applying $f_{ac} = 10kHz, 50kHz, 100kHz$ at a distance of $1\mu m$ from the junction both samples show $N_{DL,395°C} = N_{DL,380°C} \approx 5 \cdot 10^{14} cm^{-3}$, however increasing the inverse polarization of the device we observe a decrement of shallow defects down to $6 \cdot 10^{13} cm^{-3}$ after a distance of 2.7 μm. As a consequence of lower N_{DL} with the same sweep of the dc voltage (-2V, +600mV) we can investigate a wider part of the device, with the same bias the depletion region extends more in less doped semiconductor. At 1MHz we have two different effects: before $2\mu m$ shallow defects decrease like if less acceptors were active, after 2 μm shallow defects increases like if dominant defect were donor type. It seems that the transformation caused by $CdCl_2$ at 380°C is similar compared to 395°C in the first $2\mu m$ near the junction, but it is not yet complete for the whole device. Deep defect peak moves slightly farther with frequency from $1.5\mu m$ at 10kHz to $1.7\mu m$ at 100kHz and $N_{deep,380°C} = N_{deep,395°C} \approx 2 \cdot 10^{14} cm^{-3}$. At 1MHz situation is different as we observe a small peak at $1.5\mu m$ of $3 \cdot 10^{14} cm^{-3}$ and then a constant value of $2 \cdot 10^{14} cm^{-3}$ until $2.5\mu m$. So deep defects are more spread than previous cases.

4.5.4 Treatment temperature: 360°C

This sample is similar to sample made at 380°C, small distance between CV and DLCP profile, both shallow and deep defect profile are overlapped at lower frequencies (10kHz-100kHz), shallow defects are roughly the same to the one treated at 395°C until the distance $2\mu m$, farther from the junction $N_{DL,360°C} < N_{DL,395°C}$. At 1MHz DLCP profile slightly increases and shifts to the right suggesting that the dominant defect, affected by freeze out, is a donor type distributed on the whole length of the analyzed region. Deep defects peak is measured at $1.5\mu m$ for lower frequencies and has a slightly higher value than the best treatment $N_{deep,360°C} \approx 2.5 \cdot 10^{14} cm^{-3}$. Conversely at 1MHz we have a different situation, deep defects profile shifts and increases like the shallow curve does.

4.5.5 Treatment temperature: 330°C

Shallow defects are higher than the best case, for lower frequencies at $1\mu m$ $N_{DL,395°C} \approx 5 \cdot 10^{14} cm^{-3}$ while $N_{DL,330°C} \approx 9 \cdot 10^{14} cm^{-3}$. At low frequencies both CV and DLCP profiles are almost overlapped and due to a higher concentration, our voltage sweep allows to investigate the device until $1.5\mu m$. Increasing the frequency we observe the freeze out of the dominant defect as in the case of 360°C, however in the previous case shallow defects were higher and ranged between $9 \cdot 10^{13} cm^{-3}$ and $4 \cdot 10^{14} cm^{-3}$, while in this case N_{DL} ranges between $2 \cdot 10^{13} cm^{-3}$ and $6 \cdot 10^{13} cm^{-3}$. This suggest that dominant defects affected by freeze out are donor type in the former case and acceptor type in the latter case. Deep defects concentration is higher compared to the previous case and also to the best case, $N_{deep,360°C} \approx 6 \cdot 10^{14} cm^{-3}$ is detected at $1\mu m$. At 1MHz we can see that deep defects are higher, considering a distance of $2\mu m$ we observe $N_{deep,330°C} \approx 7 \cdot 10^{14} cm^{-3}$ and $N_{deep,360°C} \approx 2.5 \cdot 10^{14} cm^{-3}$.

4.5.6 Treatment temperature: 310°C

Shallow defects are slightly higher than the best case: at 10kHz and $1\mu m$ distance $N_{DL,310°C} \approx 8.5 \cdot 10^{14} cm^{-3}$ while $N_{DL,395°C} \approx 5.5 \cdot 10^{14} cm^{-3}$. Defects are slower than previous samples, N_{DL} increases at 50kHz due to a dominant donor defects, however at 100kHz shallow profiles does not follow the trend: before $1.1\mu m$ is higher than lower frequencies, after this point N_{DL} concentration is lower compared to the measurement at 10kHz and 50kHz. Increasing more the frequency we have the same situation of 330°C where freeze out occurs, in this case curve shift is higher. Deep defects concentration increases with frequency: $N_{deep,310°C} \approx 3 \cdot 10^{14} cm^{-3}$ at 10kHz and 50kHz, $N_{deep,310°C} \approx 9.5 \cdot 10^{14} cm^{-3}$ at 100kHz; all three peaks are detected around $1.2\mu m$. At 1MHz deep contribution effect shifts at $2.5\mu m$ and measures $N_{deep,310°C} \approx 1.5 \cdot 10^{15} cm^{-3}$.

4.5.7 DLCP/CV summary

Lower treatment temperature produces samples with high shallow profile but with also high deep defect concentration. Activation treatment passivates both shallow and deep defects, it is possible to change their relative concentration by changing the treatment temperature, best trade off is achieved at $395°C$. Defects capability to follow fast ac bias increases with higher treatment temperature.

At 380°C and 395°C shallow defects concentration is higher than deep defects but sample treated at the former temperature shows a contributions of donor defects while in latter case they are not presents. Moreover deep defects are more spread in sample made 380°C. This could be an explanation for a better performance of the sample treated at 395°C compared to the one made at 380°C. At 410°C performance are worse due to an increment of deep defects.

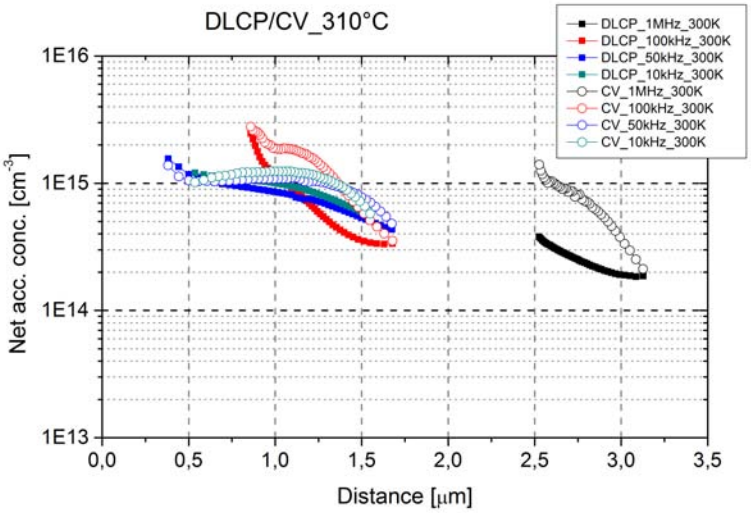

Figure 4.37: DLCP/CV at 310°C.

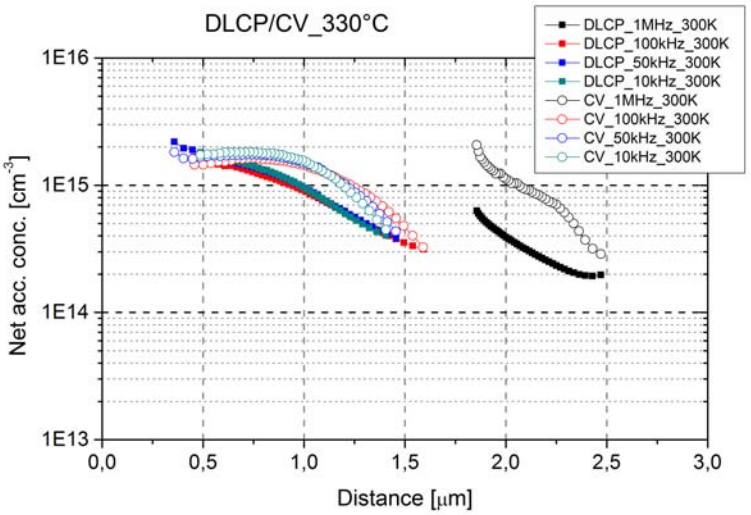

Figure 4.38: DLCP/CV at 330°C.

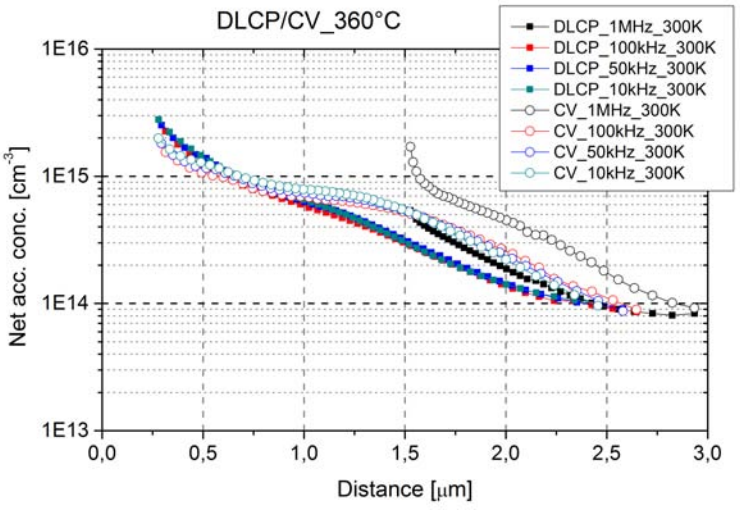

Figure 4.39: DLCP/CV at 360°C.

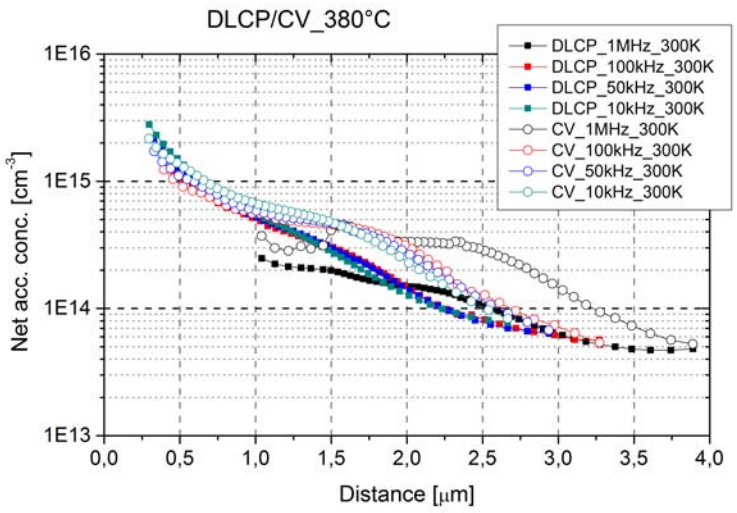

Figure 4.40: DLCP/CV at 380°C.

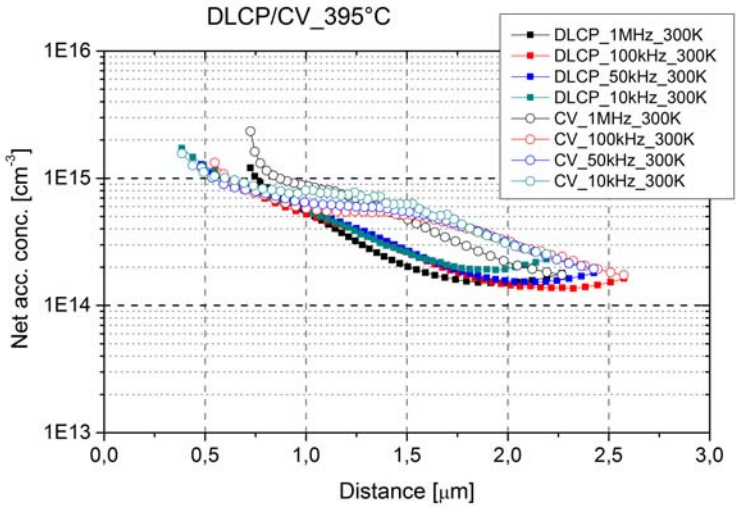

Figure 4.41: DLCP/CV at 395°C.

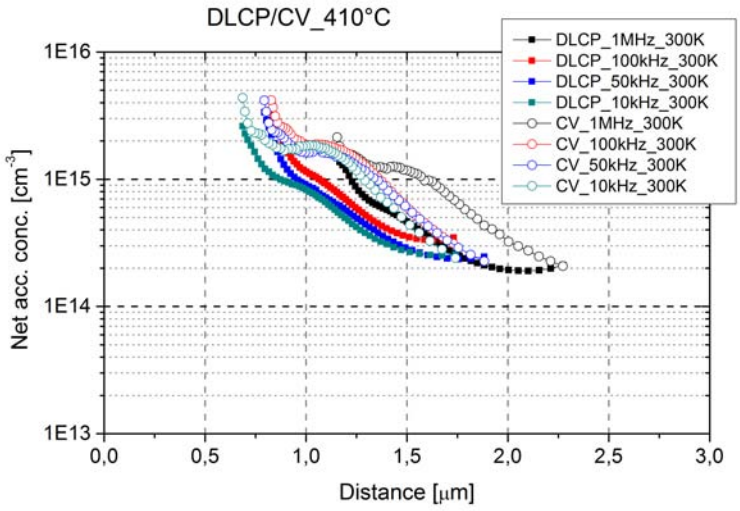

Figure 4.42: DLCP/CV at 410°C.

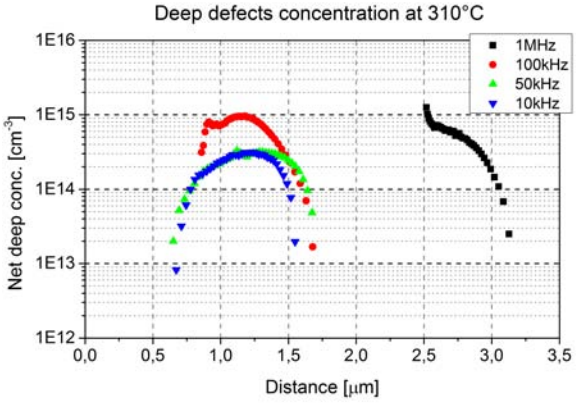

Figure 4.43: Deep defects at 310°C.

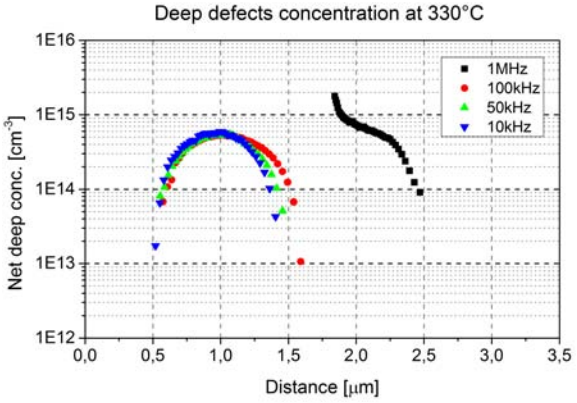

Figure 4.44: Deep defects at 330°C.

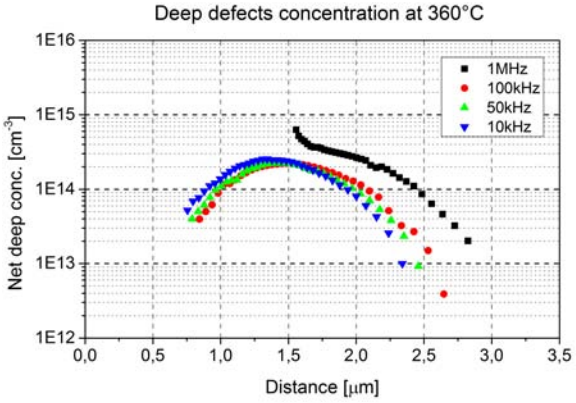

Figure 4.45: Deep defects at 360°C.

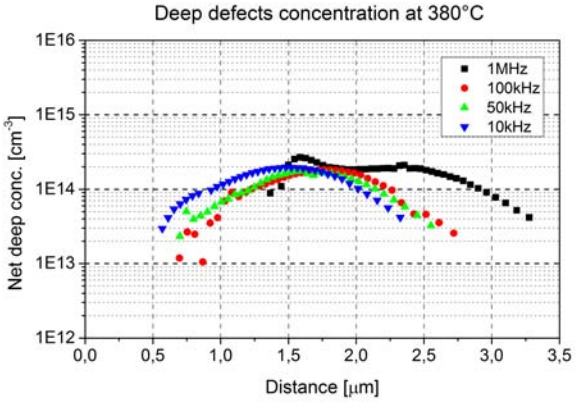

Figure 4.46: Deep defects at 380°C.

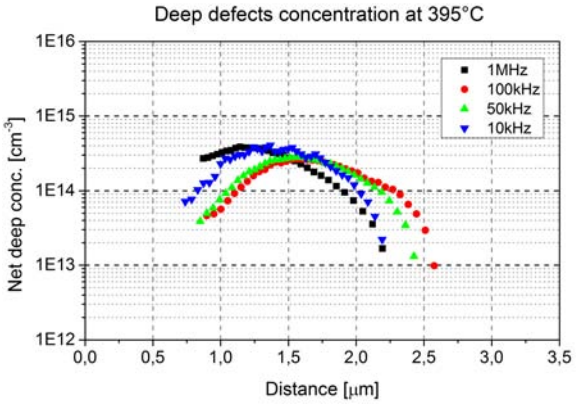

Figure 4.47: Deep defects at 395°C.

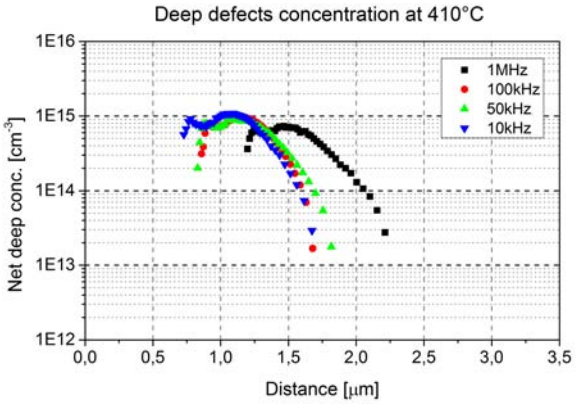

Figure 4.48: Deep defects at 410°C.

4.6 EQE

EQE measurement are performed with LOANA system described in paragraph 3.5. We can see high reproducibility of quantum efficiency curves between different cells of the same sample (figures 4.49-4.53). Lower reproducibility is observed for the sample treated at 410°C (figure 4.54) which keeps the same form of the curve but have different peak values. This confirms that activation treatment performed at 410°C spoils the film and affects inhomogeneously the CdS/CdTe junction, EQE at this temperature is clearly worse than the others. Comparison between other curves (figure 4.55) is not straightforward. The most evident effect is the drop of the EQE response at wavelength ranging between 500 nm and 600 nm. This confirms a different transformation of the window layer creating a different intermixing layer between CdS/CdTe and show that EQE worsens with temperature. Looking at cutoff wavelength between 810 nm and 870 nm we have a slightly increase of EQE with treatment temperature. Also in the center part between 600 nm and 810 nm curves made at 360°C, 380°C, 395°C, respectively green, blue and light blue are slightly higher than the black and the red curves. We also measured J_{sc} of the samples using the LOANA system and we get contradictory result with J-V shown in paragraph 4.2. All shortcut current measurements show lower values. Statistical results are reported in figure 4.56. According to this measurement best J_{sc} is achieved at 360°C. Verona laboratories measurement system uses an halogen lamp while LOANA has a flash light source more similar to solar spectrum, halogen lamp has lower emission at lower wavelengths, on the other hand LOANA system is more complex and need more calibration settings, it is possible that CdTe solar cells requires some different parameter compared to the set up used for silicon cells. Moreover LOANA probes need a PCB with spring connectors to perform the measurement. These type of connectors can damage sample surface scratching device area and reducing the solar cell active region. Hence EQE results should be investigate further more. It would be necessary to repeat measurement with more samples to have a more reliable statistic. Moreover J-V measurement with LOANA system would be very interesting to compare also fill factor, V_{oc}, efficiency.

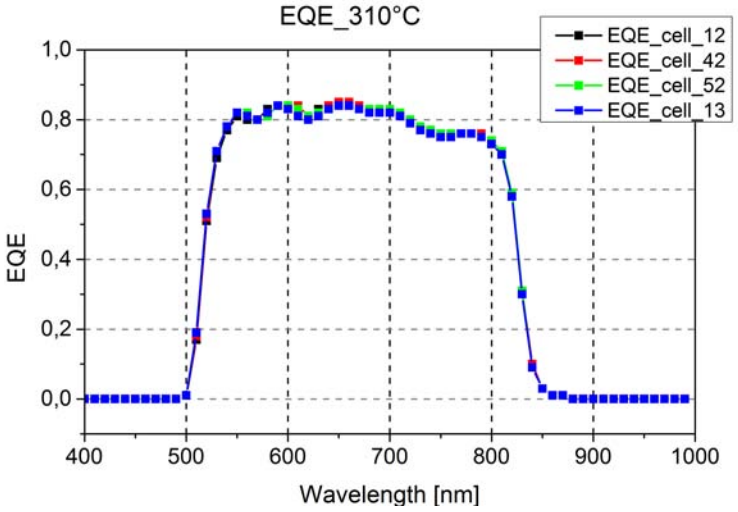

Figure 4.49: EQE at 310°C.

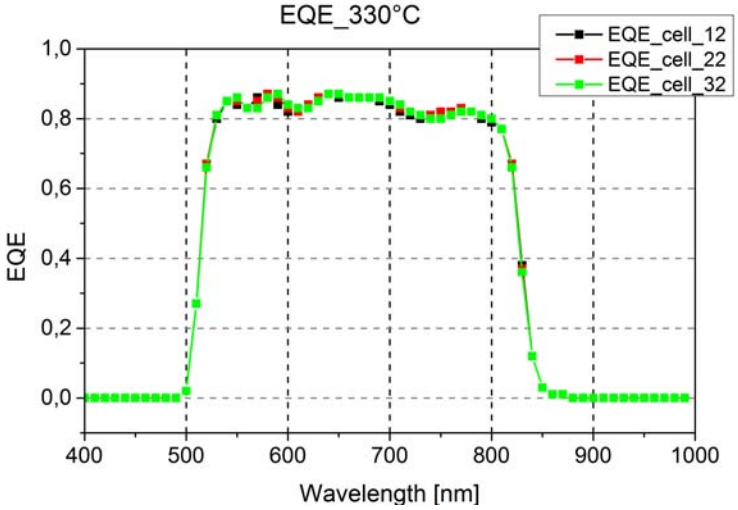

Figure 4.50: EQE at 330°C.

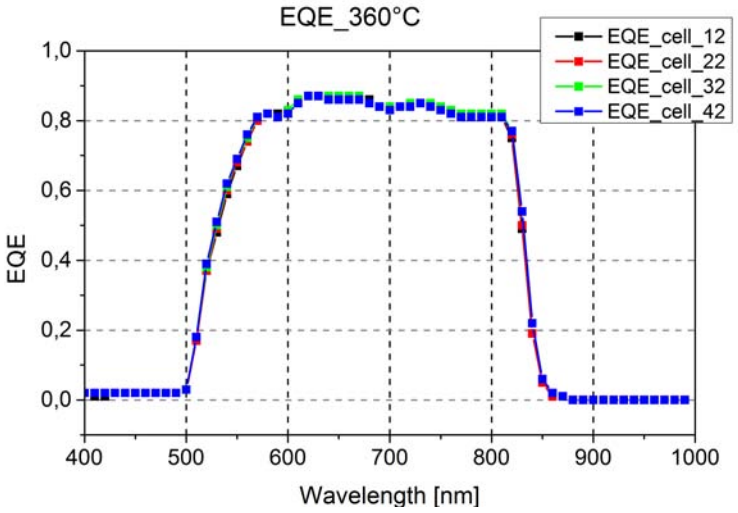

Figure 4.51: EQE at 360°C.

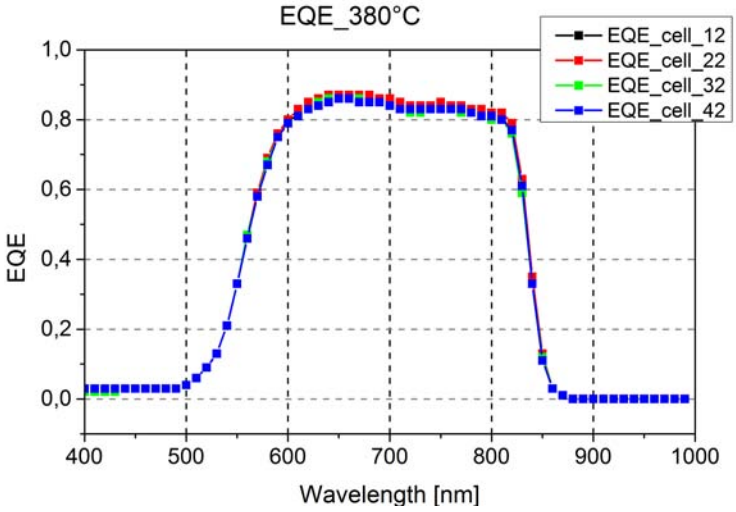

Figure 4.52: EQE at 380°C.

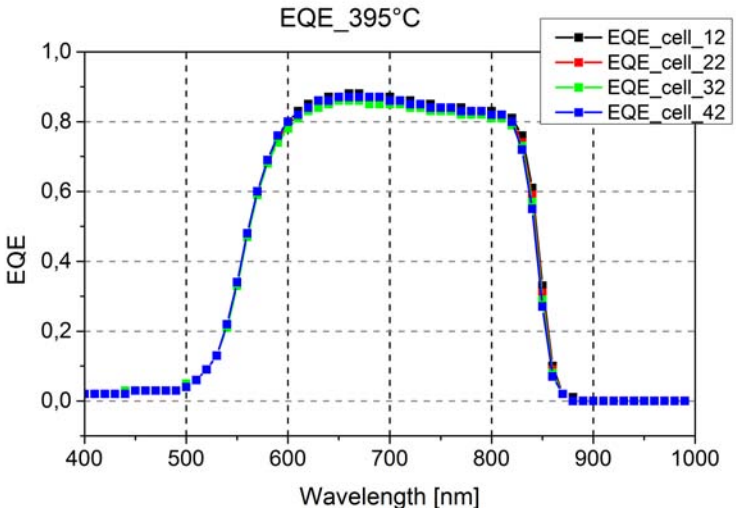

Figure 4.53: EQE at 395°C.

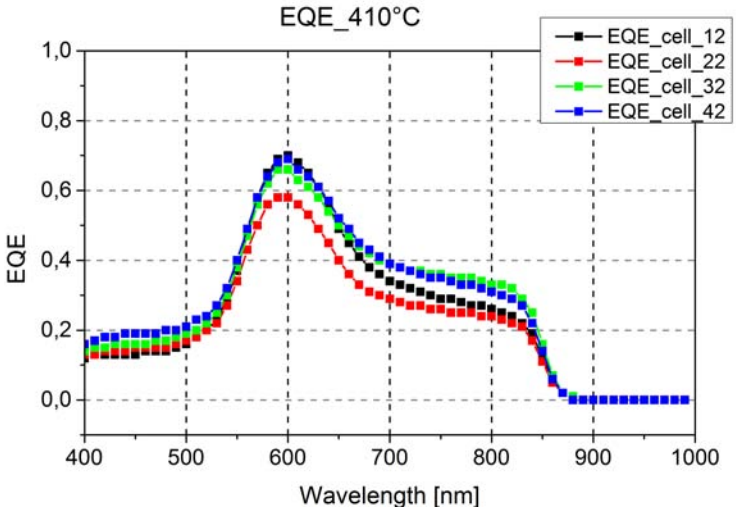

Figure 4.54: EQE at 410°C.

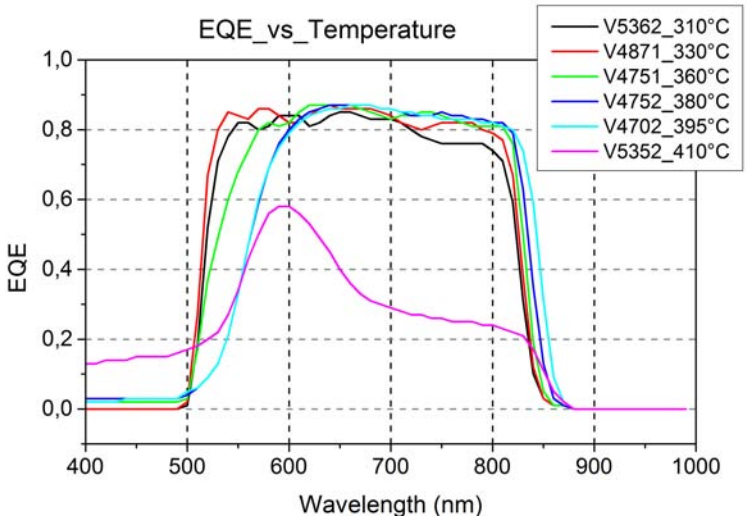

Figure 4.55: Comparison between EQE made at different treatment temperature.

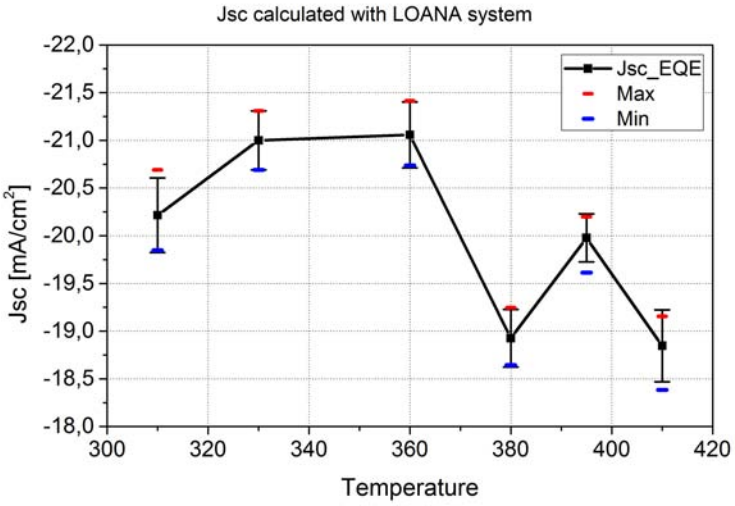

Figure 4.56: J_{sc} measured with LOANA system.

Chapter 5

Conclusions

Activation treatment step process is stabilized studying different solutions behaviour. Most of the experiments are reported in detail in chapter 2. We defined a procedure to obtain homogeneous and repeatable treatments. Stable solution has been used to study the effects of treatment temperature on the final device. Temperatures studied are 310°C, 330°C, 360°C, 380°C, 395°C, 410°C. Strong connection between V_{oc} and treatment temperature results by J-V characterization. Highest efficiency is achieved with sample treated at 395°C. Best fill factors are obtained with both 380°C and 395°C. J_{sc} values should be investigate more as contradictory results are reported between J-V measurement and data obtained at Padua laboratories. It is worth to underline that fewer samples were measured with LOANA compared to samples measured with J-V, hence more samples should be measured at Padua laboratories to have a reliable statistics. Surely measurement discrepancy are not negligible and worth to investigate deeply both measurement set up. J-V measurement with LOANA system would be interesting to compare other parameter such as efficiency, V_{oc}, fill factor. Probably sample made at 395°C would reach highest efficiency also with LOANA measurements. XRD patterns show that CdTe when deposited in vacuum chamber has (111) preferred orientation, $CdCl_2$ treatment induces crystallographic rearrangements in CdTe layer, its effectiveness increases with temperature. Also lattice parameter changes with temperature and stays constant at 360°C, 380°C and 395°C that are the temperatures with higher efficiencies (over 13%). CdTe grains size also increases with temperature that is surely positive. CV and DLCP show that both shallow and deep defects concentration are higher in samples treated at lower temperatures. Best tradeoff is achieved at 395°C where shallow defects concentration is higher than deep defects. EQE shows that intermixing changes with temperature as lower wavelengths response sensibly decrease, nevertheless at higher wavelengths we have slightly higher values of EQE. In conclusion activation treatment is responsible of many transformation in CdS/CdTe structures that can be both positive or negative. Samples made at 395°C have the best tradeoff and can reach higher efficiencies than samples made at the other temperatures.

Bibliography

[1] Alessandro Romeo, *Growth and Characterization of High Efficiency CdTe/CdS Solar Cells*, PhD thesis, 2002.

[2] Ivan Rimmaudo, *Study of structure and electronic properties of high performance CdTe solar cells by electrical invstigation.*, PhD thesis, 2013.

[3] Andrei Salavei, *New Fabrication Approaches for High Efficiency CdS/CdTe Solar Cells*, PhD thesis, 2013.

[4] Jef Poortmans and Vladimir Arkhipov *Thin Film Solar Cells. Fabrication, Characterization and Applications*, Wiley 2006

[5] Jennifer T. Heath, J. David Cohen, William N. Shafarman, *Bulk and metastable defects in $CuIn_{1-x}Ga_xSe_2$ thin films using drive-level capacitance profiling*, Journal of Applied Physics, Volume 95, number 3, 2004.

[6] Richard S. Muller and Theodore I. Kamins with Mansun Chan, *Device Electronics for Integrated Circuits*, Wiley, 2003.

[7] J. B. Nelson and D. P. Riley *An experimental Investigation of Extrapolation Methods in the Derivation of Accurate Unit-Cell dimensions of Crystals*, Cavendish Laboratory, Cambridge, 1944.

[8] H. R. Moutinho, M.M. Al-Jassim, F.A. Abufoltuh, D.H. Levi, P.C. Dippo, R.G. Dhere and L.L. Kazmerski, *Studies of Recrystallization of CdTe Thin Films After $CdCl_2$ Treatment*, 26th IEEE Photovoltaic Specialist Conference (September 29 - October 3, 1997, Anaheim, California), NREL, Colorado, 1997.

[9] M. Burgelman, P. Nollet, S. Degrave *Electronic behaviour of thin film CdTe solar cells*, Applied Physics A, Materials Science & Processing, 1999.

[10] M. Gloeckler, A.L. Fahrenbruch, and J.R. Sites *Numerical Modeling of CIGS and CdTe Solar Cells: Setting the Baseline*, 3rd World Conference on Photovoltaic Energy Conversion (May 11-18, 2003, Osaka, Japan), Colorado State University, 2003

Prima di chiudere il capitolo Università sento il bisogno di ringraziare tutti coloro che fanno o hanno fatto parte della mia vita.
Mio nonno che da lassù gioisce e si commuove nel vedermi Ingegnere, mia nonna che mi ama come un figlio e mi ha guidato nella vita fino ad oggi.
Ringrazio mamma e papà che ogni giorno fanno tanti sacrifici per me e la mia sorellina, Lei Pin. Grazie Zapon e Canna e Dewei perchè siete troppo forti ed è bellissimo vivere insieme a voi.
Grazie a tutti gli amici di Lodi con cui mi sono divertito per anni, siete lontani ora, ma le ore passate in via Ferrabini e alla Faustina saranno sempre vivi nei miei ricordi.
Agli amici di Verona che mi volete bene anche se ho sempre poco tempo da trascorrere con voi ma quando c'è da divertirsi si riesce sempre ad organizzare in qualche modo (cioè che io vi raggiungo appena finisco...) Siete mitici!
Ai Padovani anche se in realtà praticamente nessuno è di Padova. Grazie a tutto il gruppo mensa, son nove mesi che sono in lab a Verona e ogni giorno mi tenete aggiornato su dove e quando andate a mangiare. Un grazie speciale a mastro Celin che pur non essendo capace di scegliere gli esami, non ha mai detto di no a un "Ti posso chiamare?"... La Vodafone ha già licenziato gli idioti che hanno inventato la tariffa col numero preferito.
Grazie a tutta la ciurma del LAPS, ad Alessandro che mi ha permesso di lavorare nel suo fantastico laboratorio, a Ivan e Andrei per avermi insegnato due metodi diversi di fare Scienza "senza esagerare!". Grazie a Marelsa perchè sarebbe stato faticoso gestirli da solo... Grazie anche alle new entries del lab Zimoone e l'africano che hanno il dovere di sostituire al meglio il rasta, il cinese e la bionda nella barzelletta della mensa. È stato bello imparare con voi.
Grazie a Mario, Daniela, Silvia e Pietro per tutto quello che abbiamo condiviso, lo slittino estivo, il mare, l'interspar e le preghiere.

Grazie a te Prisca, la mia Prisca, che rendi speciale ogni attimo della mia vita. È stato un dono incontrarti, è un dono viverti. Questa gioia che condividiamo oggi è solo un piccolo morso del nostro futuro insieme.